12-2009

INVESTIGATION OF THE THERMOELECTRIC BEHAVIOR AND STRUCTURE FORMATION OF (PbTe/AgSbTe2)-SILVER CHALCOGENIDE MIXTURES

Yisha Wang
Clemson University, yishaw@clemson.edu

INVESTIGATION OF THE THERMOELECTRIC BEHAVIOR AND STRUCTURE FORMATION OF ($PbTe/AgSbTe_2$)-SILVER CHALCOGENIDE MIXTURES

A Thesis
Presented to
the Graduate School of
Clemson University

In Partial Fulfillment
of the Requirements for the Degree
Master of Science
Material Science and Engineering

---

by
Yisha Wang
December 2009

Accepted by:
Dr. Fivos R. Drymiotis, Committee Chair
Dr. Terry M. Tritt
Dr. Philip Brown
Dr. Jian Luo
Dr. Bogdan Zdyrko

ABSTRACT

Sustainable energy research is currently on the forefront of scientific exploration and energy conservation and the development of new energy production techniques are both crucial for our long lasting stable future. Accordingly, thermoelectric materials will be a significant energy conservation and production source. The state-of –the-art thermoelectric materials can be used to collect the wasted heat and converted to power, which is the future for the green power generation.

PbTe is considered a state-of-the-art thermoelectric material, which has been extensively studied. It forms in the NaCl structure and it is a semiconductor with a room temperature gap value of 0.29 eV. Ag and Se was chosen to dope into the PbTe system to form (PbTe)(Ag_xSe). The hope was that the presence of nano-scale inhomogeneities would lead to a significant reduction in the thermal conductivity and a significant improvement of the thermoelectric Figure-of-merit with respect to the stoichiometric PbTe. With the result of PbTe (Ag_xSe), the similar system $Cu_xAg_{3-x}SbSeTe_2$ alloy were doped to further reduce the thermal conductivity and improve the Figure-of-merit ZT.

DEDICATION

I dedicate this work to the greatest love of my life – my parents.

ACKNOWLEDGMENTS

I would first like to thank Dr. Fivos Drymiotis for accepting me to be a member of his group. He is so nice, helpful, kind and supportive. He has been my greatest source of insight, knowledge, and direction. Also, he has been a great help in assisting me in planning my life. I learned lots from him, not only for academic, but also for being a nice person.

A special thanks to Dr. Terry Tritt and Dr. Jian He for helping me.

In addition, I would like to thank all the group members in Dr.Drymiotis' and Dr. Tritt's groups. Without their help, it's impossible for me to finish my project.

TABLE OF CONTENTS

Page

LIST OF FIGURES

CHAPTOR ONE

INTRODUCTION

Thermoelectrics

Thermoelectric materials gained popularity as a research field during the 1990s. [1] The interest was driven by the need for more efficient materials for electronic refrigeration and power generation applications.[2] Thermoelectric effects are related to the conversion between thermal and electrical energy. Thermoelectric refrigeration is an environmentally "green" method of small scale cooling, applied in computers, infrared detectors, electronics, and other applications as well.[3] The first prototype thermoelectric refrigerator was constructed in 1953.[3]

Due to the present global energy shortage and predicted increase in future energy demands, there is a more pressing need to develop a technology which will enable an alternative energy conversion and transition to the post-fossil fuel era. Thermoelectric materials for power generation are an important method to solve the energy problem, such as the thermal to electrical energy conversion from natural heat gradients and developing electrical power generation from waste engine heat from the automotive industry.[3]

Seebeck Effect.

The thermoelectric (TE) behavior was first discovered by Thomas Johann Seebeck in the early 1800s. [1] At that time, Seebeck observed that if two dissimilar materials were joined together, and the junctions were held at dissimilar temperatures forming a temperature difference, a voltage would be produced as shown in Figure 1.1. The ratio of the voltage to the temperature gradient is an intrinsic property of a material, called the Seebeck coefficient or thermopower. [4] The temperature gradient across the materials is transferred to the electrons

in the conducting band, which causes a no-equilibrium condition in terms of energies of the conducting electrons. The electrons will move from the hot to the cold side of the material according to the Second Law of Thermodynamics. [4] Because of the unequal distribution of charge, a voltage proportional to the temperature gradient is established. In equilibrium, this new distribution of charge will establish an opposing electric field to prevent further charge diffusion. Figure 1.1 shows a basic thermoelectric circuit. The Seebeck coefficient is defined by

$$\Delta V = \alpha \Delta T$$

where V is the voltage produced, α is the Seebeck coefficient and ΔT is the temperature gradient. The sign of the Seebeck coefficient usually indicates the type of carriers present in the material. A positive Seebeck coefficient indicates that the primary carriers are holes, while a negative one indicates that electrons are dominant carriers.

Peltier Effect.

The Peltier effect bears the name of Jean-Charles Peltier (a French physicist) who discovered it in 1834.[1,5] The Peltier effect is the reverse of the Seebeck effect. It is the reversible exchange of heat from a junction of dissimilar materials in the presence of a current passing through the junction, which is held at a constant temperature.[5] When a current is passed between two dissimilar materials, heat will either be expelled or absorbed at this junction depending on the differences between the Fermi energies of the two materials as shown in Figure1.2.[2] If the current goes from a material with a higher Fermi energy to a material with a lower one heat is given off, and the converse is true. The rate that the Peltier heat is liberated or rejected at the junction is given by:

$$Q = \Pi I$$

where Π is the Peltier coefficient and I is the current through the junction. This effect generates the refrigeration application of a thermoelectric material.

Thomson Effect

In 1851, Thomson predicted the cooling or heating of a homogeneous conductor resulting from the flow of electrical current with the presence of a temperature difference, which is known as the Thomson effect.[2,6] The Thomson relation gives us the relationship between the Seebeck and Peltier effect,

$$\Pi = \alpha T$$

where Π is the Peltier coefficient, α is the Seebeck coefficient, and T is the temperature.

Thermoelectric Refrigeration and Power Generation Devices

According to the Seebeck effect and Peltier effect, the thermoelectric materials can be used for refrigeration and power generation.[7] Figure 1.3 shows a component of the thermoelectric energy conversion module. In the refrigeration mode, the Peltier effect is utilized and an external battery pushes the electrons and holes away from the cold side of the device, which results in cooling.[2] On the other hand, in the power generation mode, the Seebeck effect is utilized. A temperature gradient is applied across the module and consequently a voltage develops across the *n* and *p* legs as the heat is converted into electrical power.

The thermoelectric module has alternating n-type and p-type semiconducting materials connected by electrical contact pads.[2] The n and p semiconductors are connected electrically in a series and thermally in parallel. Figure 1.4 shows a common thermoelectric module which can operate either in refrigeration or power generation mode.

Thermoelectric devices are environment friendly, stable and do not contain moving parts. Without consuming fossil energy and producing toxins or waste, thermoelectric devices generate power or act as refrigerators.[7] However, the efficiency of the materials remain low so the cost of production versus energy savings must be taken into account. Current applications include waste heat recovery in power plants, cooling chips in computers and commercial thermoelectric coolers.

Figure of Merit

The efficiency of the thermoelectric material is determined by the dimensionless figure of merit, ZT, defined as: [2]

$$ZT = \frac{\alpha^2 \sigma}{\kappa} T = \frac{\alpha^2 T}{\rho \kappa}$$

where α is Seebeck coefficient, also called the thermopower, σ the electrical conductivity, ρ the electrical resistivity, and κ the total thermal conductivity, which is the sum of the electrical contribution (κ_e) and the lattice contribution (κ_l):

$$\kappa = \kappa_e + \kappa_l$$

The power factor is another useful parameter that is typically optimized as a function of carrier concentration through doping to give the largest ZT. [2,8]

$$Power\ Factor = \alpha^2 \sigma T = \frac{\alpha^2}{\rho \kappa}$$

Figure 1.5 shows the ZT as a function of temperature for several bulk thermoelectric materials.[9]

Thermoelectric Materials

The electrical conductivity, which is a reflection of charge carrier concentration, is one of the parameters that are used in the classification of material. According to the electrical conductivity, materials are classified into metals, semiconductors and semimetals, and insulators.[9,10] Metals have a high electrical conductivity while in insulators the conductivity is very low and under normal conditions is taken as zero; semiconductors occupy an intermediate position.[10] The electrical conductivity typically increases with increasing carrier concentration (Figure1.6) but unfortunately the Seebeck coefficient decreases.[10] The power factor consequently has a maximum at a carrier concentration of around $10^{19}/cm^3$, which is a typical carrier concentration in semiconductors. [10] Because of the low carrier concentration in semiconductors, the electronic contribution to the heat capacity is reduced as well, which implies that semiconductors are materials most suitable for thermoelectric applications.

Project goal

Sustainable energy research is currently on the forefront of scientific exploration and energy conservation and the development of new energy production techniques are both crucial for our long lasting stable future.[2,3] Accordingly, thermoelectric materials will be a significant energy conservation and production source. The state-of-the-art thermoelectric materials can be used to collect the wasted heat and converted to power, which is the future for the green power generation.

PbTe is considered a state-of-the-art thermoelectric material, which has been extensively studied. It forms in the NaCl structure and it is a semiconductor with a room temperature gap value of 0.29 eV.[10-12] Ag and Se was chosen to dope into the PbTe system to form (PbTe)(Ag_xSe). The hope was that the presence of nano-scale inhomogeneities would led to a

significant reduction in the thermal conductivity and a significant improvement of the thermoelectric figure of merit with respect to the stoichiometric PbTe.[11] With the result of PbTe (Ag_xSe), the similar system $Cu_xAg_{3-x}SbSeTe_2$ alloy was doped to further reduce the thermal conductivity and improve the Figure-of-merit ZT.

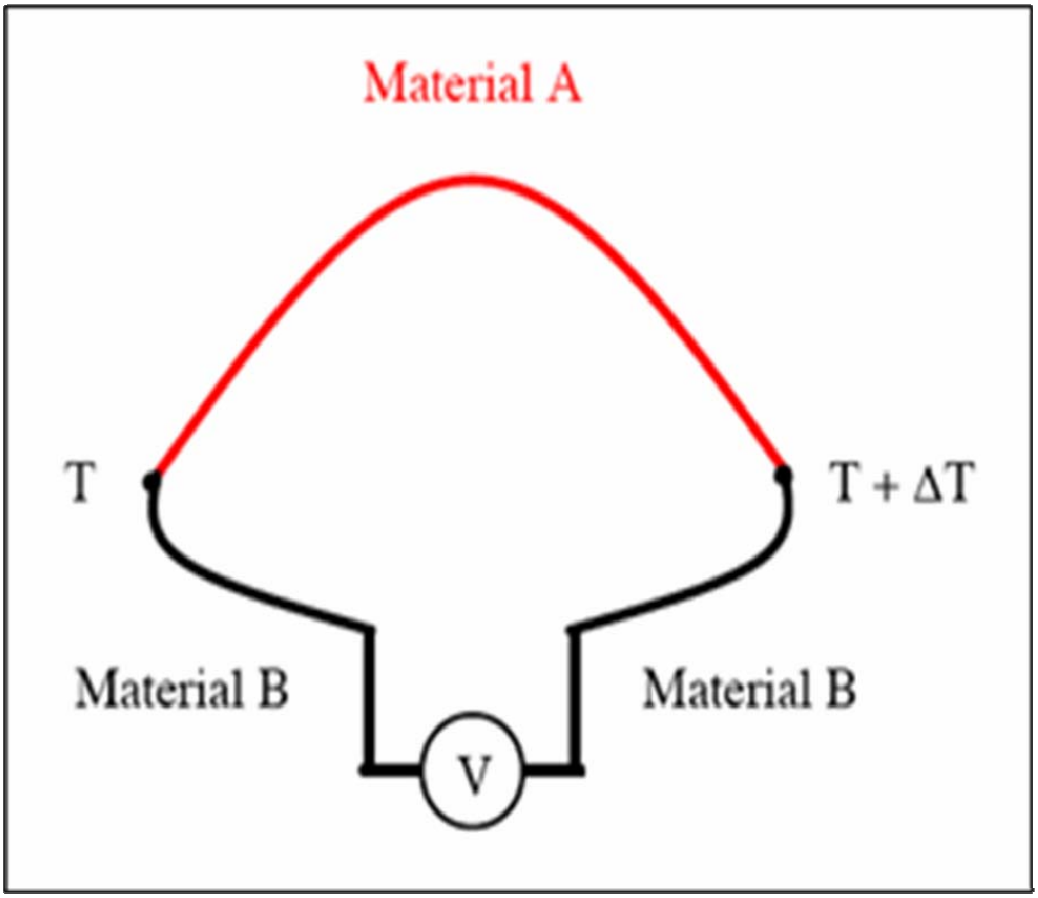

Figure 1.1 Seebeck effect

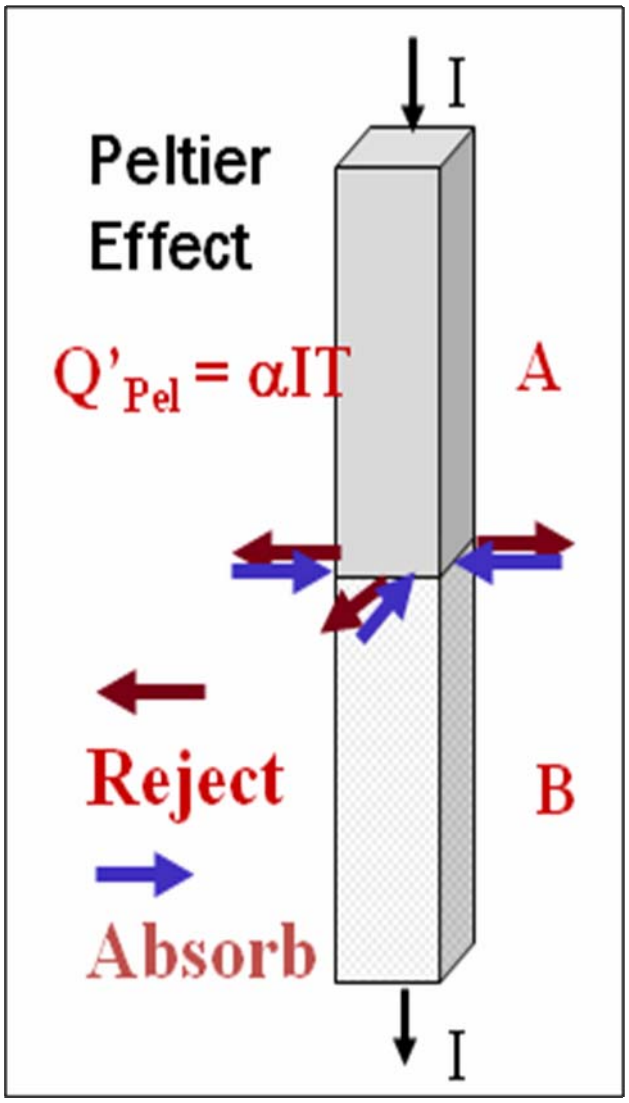

Figure 1.2 Peltier effect

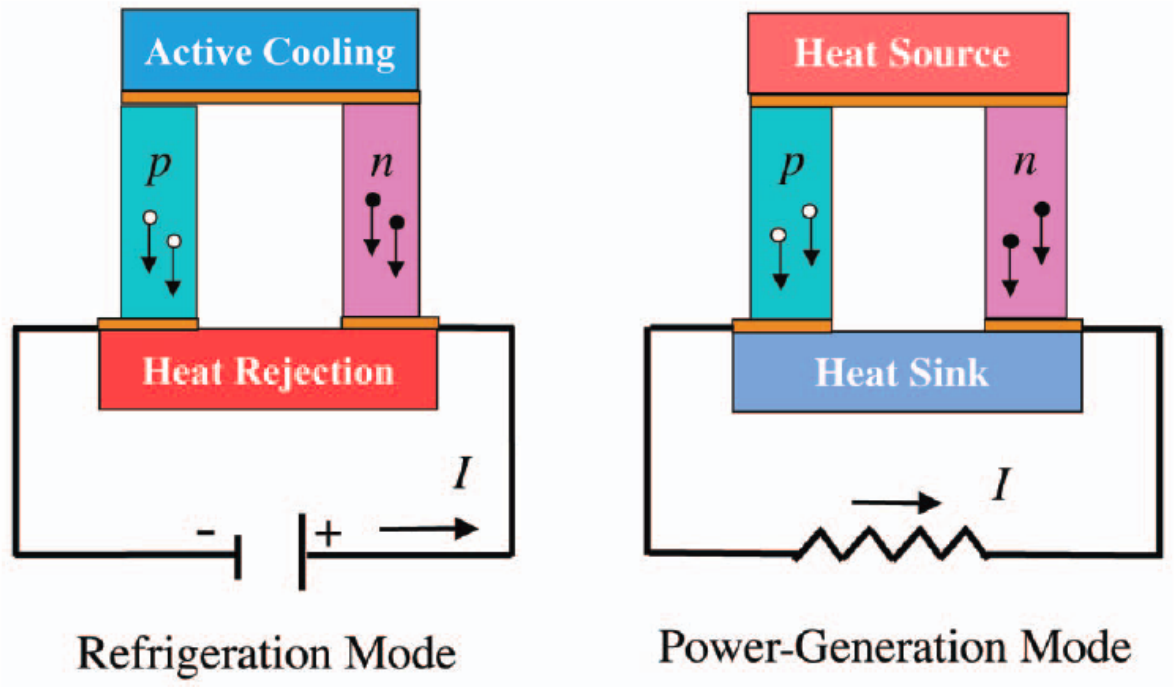

Figure 1.3 Thermoelectric couple

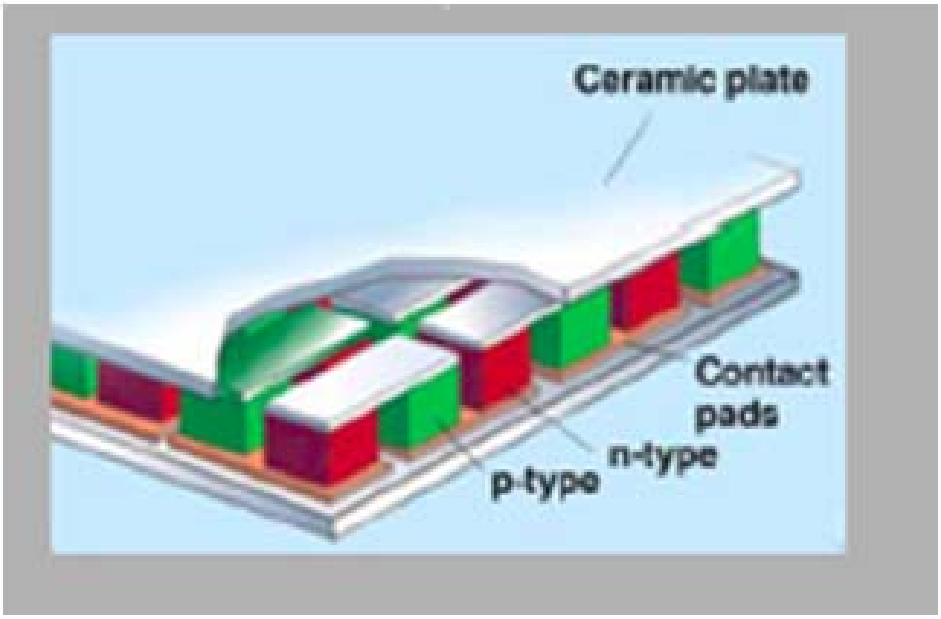

Figure 1.4 Thermoelectric Module

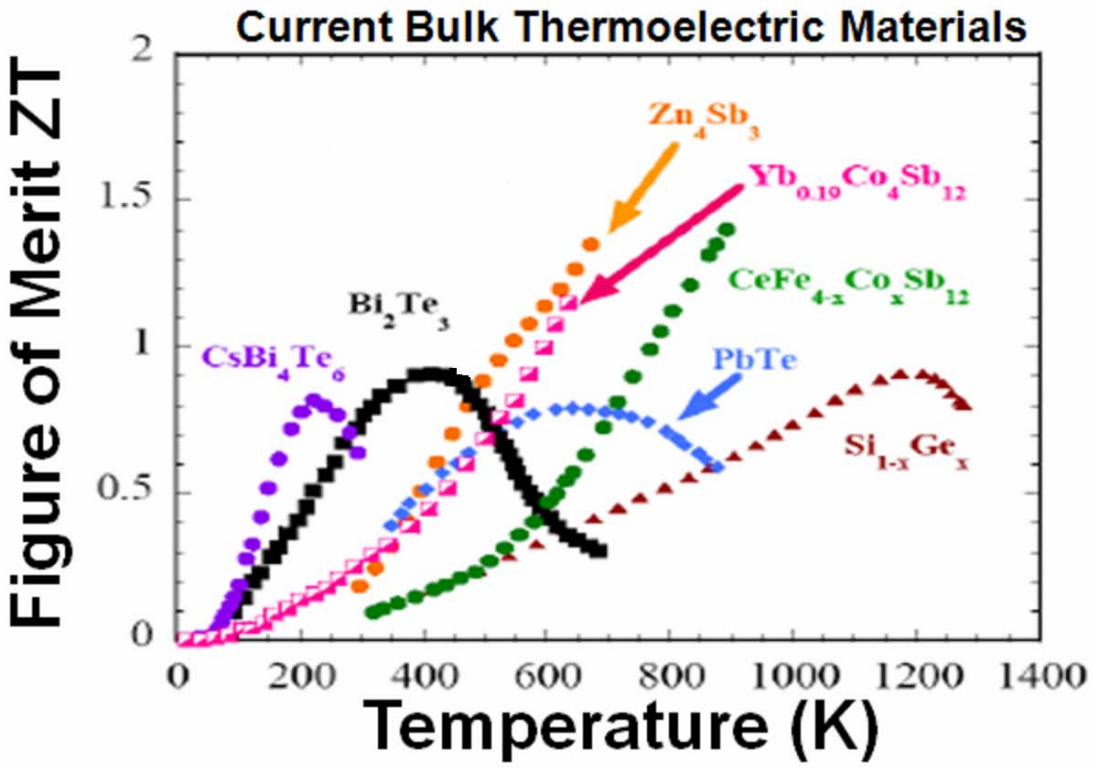

Figure 1.5 The Figure of merit ZT versus Temperature

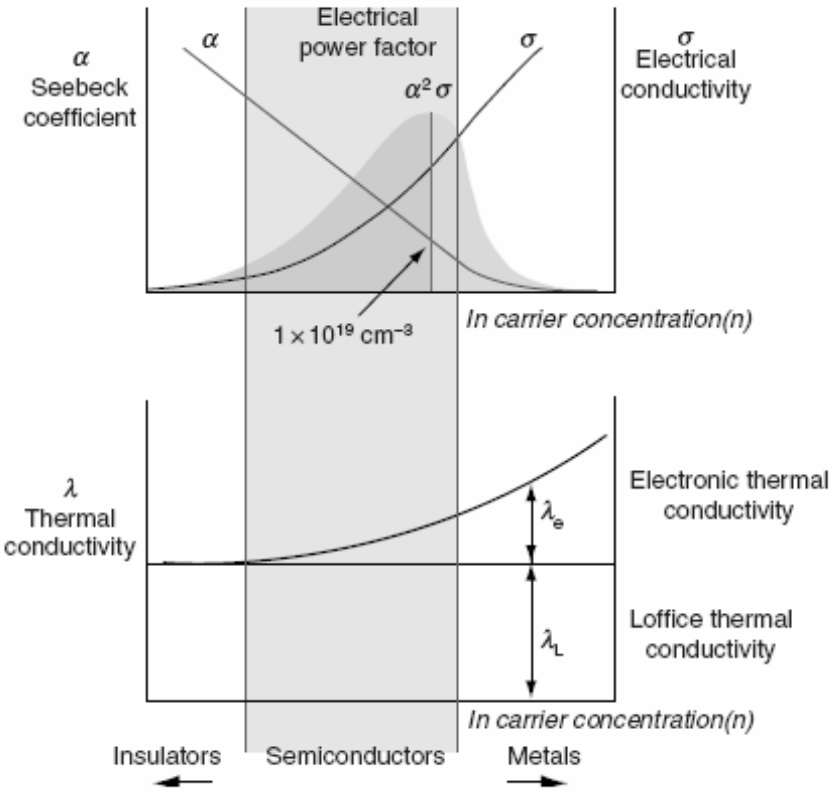

Figure 1.6 Schematic dependence of electrical conductivity, Seebeck coefficient, power factor, and thermal conductivity on concentration of free carriers.

CHAPTOR TWO

Synthesis and Measurement

Sample Synthesis

The samples used in this study were synthesized by Tyler B Drye, Daniel Rhodes, Kimberly Modic, Samantha Cawthorne, Qiu Zhang and Ben Ma, under the supervision of Dr. Fivos Drymiotis.

Synthesis of Pb:Te:Ag:Se mixtures

Pb, Te, Ag and Se with respective purities of 99.9999%, 99.9999%, 99.9999% and 99.999% were weighted and placed in quartz tubes in stoichiometric ratios 1:1:x:1, with x=1.9, 2.0, 2.01 and 2.02. The quartz tubes were evacuated, sealed and placed inside a furnace.[11] The furnace was programmed to heat to 1000 ^{o}C and the sample was held at this temperature for 4 hours, before finally allowed to cool down to 500 ^{o}C at a rate of 10 ^{o}C/hour.

Synthesis of CuxAg3-xSbSeTe2

Ag, Cu, Sb, Te, Se with respective purities of 99.9999%, 99.9999%, 99.9999%, 99.9999% and 99.999% were placed in quartz tubes in stoichiometric ratios 3-x:x:2:1, with x=0,0.1,0.2. The quartz tubes with materials inside were evacuated before putting into a box furnace. The furnace was set up to heat to 1000 ^{o}C and held for 4 hours before the furnace was turned off. Then the samples were designed to cool down to 500 ^{o}C at a rate of 10 ^{o}C/hour. For each ingot from the synthesis process, the mass was around 20 grams, with

highly dense and good mechanical properties. The density of all samples was approximate 7.3 gr/cm^3.[12]

SPS(Spark Plasma Sintering)

SPS, (Figure 2.1, Figure 2.2) also known as Field Assisted Sintering Technique (FAST) or Pulsed Electric Current Sintering (PECS), is a novel sintering technique. The process is used for enhanced densification of powders by the application of an electrical discharge combined with resistance heating and pressure. The powdered sample is placed inside a graphite dye and heated by passing pulsed DC current through the dye and the sample. The heat is generated internally which facilitates very high heating and cooling rates. The speed of the process maintains the nanostructuring of the powder, making the SPS technique a valuable tool in thermoelectrics research.

After the sample was ball milled, the SPS was applied to them. The sample was taken out of the furnace after the furnace cooled down to room temperature. The sample was taken out from the quartz tube and cut into several discs. One of the discs was ball milled to get significantly fine powder. The powder was placed in the die in the sample chamber. The samples were SPS at two different temperatures, 400 ^{o}C and 500 ^{o}C.

Thermal Transport Properties Measurement

High Temperature Thermal Conductivity

The high temperature thermal conductivity was calculated using the density of the sample ρ, its heat capacity at constant pressure C_p, and its diffusivity D. A Differential Scanning Calorimeter (DSC) (Figure 2.3, 2.4) was used to measure the heat capacity of the sample at a

constant pressure, and a Laser Flash (Figure 2.5, 2.6) was used to measure its thermal diffusivity. The thermal conductivity was then calculated using the following equation:

$\kappa = \rho\, C_v\, D \approx \rho\, C_p\, D$

Low Temperature Specific Heat Capacity

The low temperature specific heat capacity was taken on the commercial Physical Properties Measurement System (PPMS) (Figure 2.7) by Dr. J. Lashey in Los Alamos National Laboratory.

Low Temperature Thermal Conductivity

Low temperature thermal conductivity was also measured using a steady-state thermal conductivity measurement system. The home built system uses a helium cryo-cooler and has the capability of reaching temperatures below 10 K. Two samples can be simultaneously mounted on a removable puck.[14] Samples were mounted on individual pucks as shown in Figure 2.8 and measured simultaneously in a vacuum of 10^{-3} torr and with the temperature ranging from 10 K to 300 K. [14] The thermal conductivity mounting system is shown in Figure 2.9, while Figure 2.10 shows the low temperature thermal conductivity cryo-cooler and accompanying equipment. [14]

Electrical Transport Properties Measurement

High Temperature Resistivity and Seebeck

A commercial Model ZEM-2 Seebeck Coefficient/Electric Resistance Measuring System (Figure 2.11) was used to measure high temperature Seebeck and resistivity. Figure 2.12 shows the detail of the Probe Head and the sample mounting for measurement purposes.[15]

The system can measure up to 800 ^{o}C in a low pressure inert atmosphere. To get accurate data, samples were prepared in the shape of a prism with dimension approximately 2× 2× (6-8)mm^3. In addition, each surface of the sample was polished before measuring and both end surfaces of the samples were parallel to each other. There were two thermocouples attached to each probe head which read absolute temperature and also measured the temperature difference across the sample.[15] Similarly, there was another thermocouple which was placed outside a metallic shield during the measurement. The whole measurement was placed inside an Argon atmosphere.

Low Temperature Resistivity and Seebeck

Resistivity and Seebeck coefficient were determined simultaneously from temperature ranges approximately 10K to 300K with a custom-designed helium cryocooler system.[16] The entire system (Figure 2.13) was controlled by a computer running Labview and the samples were run in a vacuum of 10^{-3}. The combination of automated computer control and dual sample mounts drastically reduced the amount of measurement time for each sample. In this system, the samples needed to mount on a specially designed mounting chip, which is shown in Figure 2.14. Samples were individually mounted on this 24-pin chip and plugged into the system. During the measurement, the current ran through one pair of leads (I^+,I^-) and the voltage was determined by the other pair (V^+,V^-). A pair of thermocouples were embedded in two copper blocks.[16] One junction of the thermocouple was embedded in a small copper block, and the other junction was embedded into a bigger copper block. Both of the two copper blocks were soldered to the two ends of the sample. The thermoelectric voltage (V_{TE}) was determined by a different set of voltage leads attached to the copper block.

Sample Characterization

X-Ray Diffraction (XRD)

The X-Ray diffraction system was used to characterize the purity of sample crystals. The XRD used in CAML is a compact MiniFlex x-ray diffraction system (Figure 2.15). It is equipped with an automatic sample changer which allows it to produce high resolution x-ray diffraction data up to six samples in a row without manually changing samples.

Scanning Electron Microscopy (SEM)

The SEM images were taken in Electron Microscope Facility at Clemson University Research Park. FESEM-Hitachi S4800 (Figure 2.16), equipped with an Oxford INCA Energy 200 EDS and GW Electronics Centaurus backscatter detector, was used to take high resolution microscopy images. SEM3400 S-3400N (Figure 2.17) was also used to take the image of the samples. It is equipped with Oxford INCA EDS, WDS, EBSD and a built-in four quadrant solid-state backscattering detector.[17]

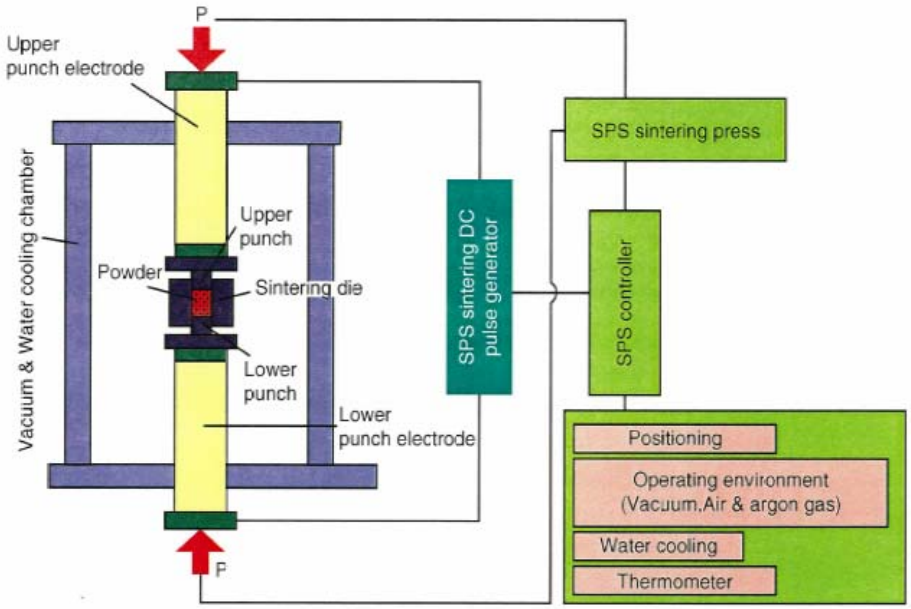

Figure 2.1 SPS system

Source: http://www.kompas.or.kr/mail/200311/tech_doc/equip02.jpg

Figure 2.2 SPS equipment

Figure 2.3 DSC equipment [13]

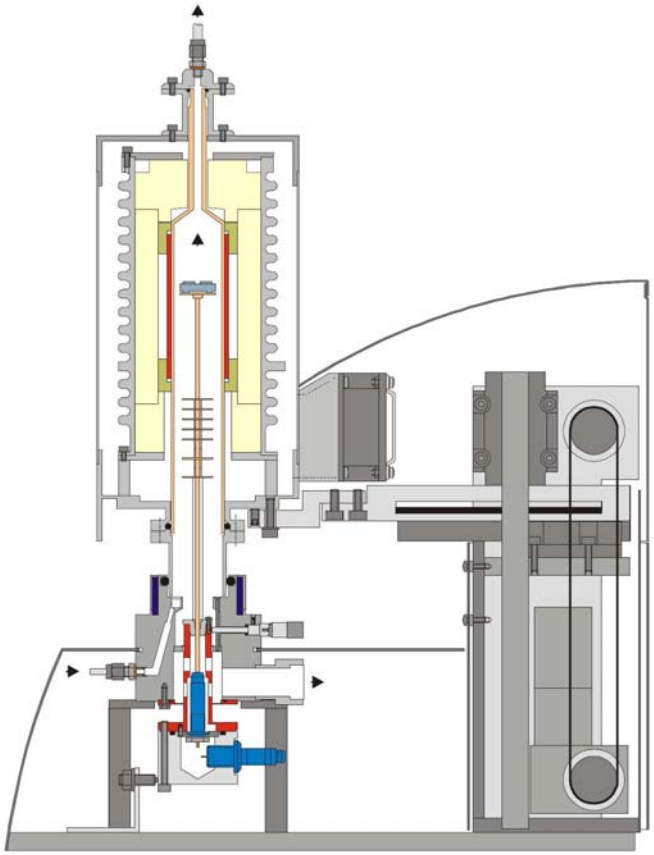

Figure 2.4 Netzsch DSC 404 C Pegasus
Source: Netzsch "DSC 404 C Pegasus System Components"

Figure 2.5 Laser Flash Equipment[13]

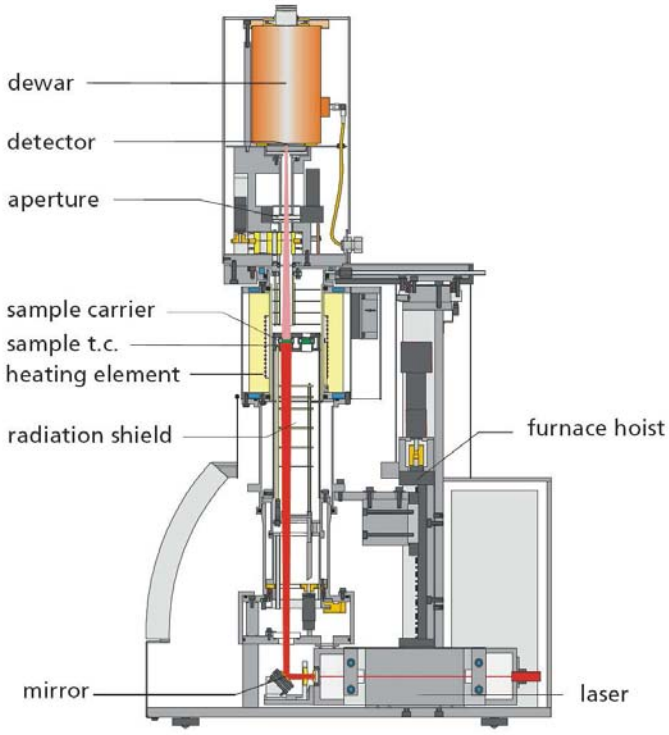

Figure 2.6 Netzsch LFA 457 Microflash
Source: Netzsch "Operating Instructions: LFA 457 Microflash"[18]

Figure. 2.7 Physical Property Measurement System[13]

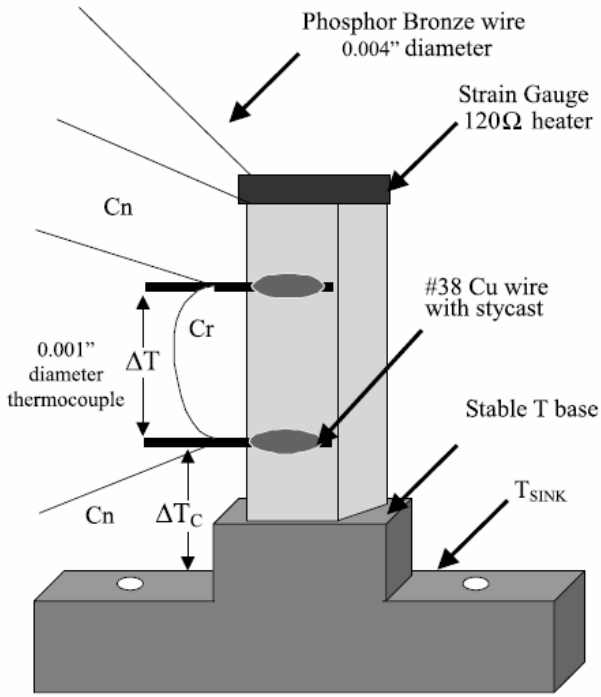

Figure 2.8 Low TC sample mounting on puck[14]

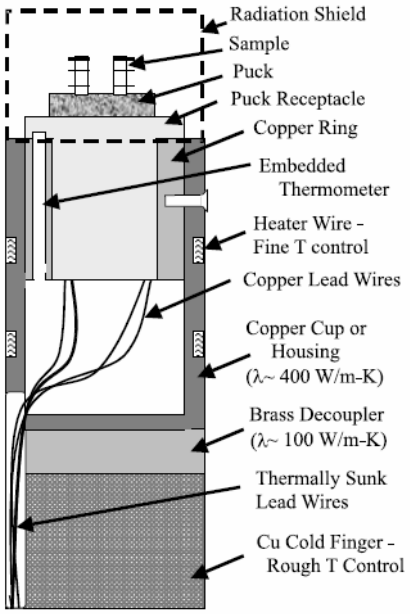

Figure 2.9. Removable thermal conductivity mounting system[14]

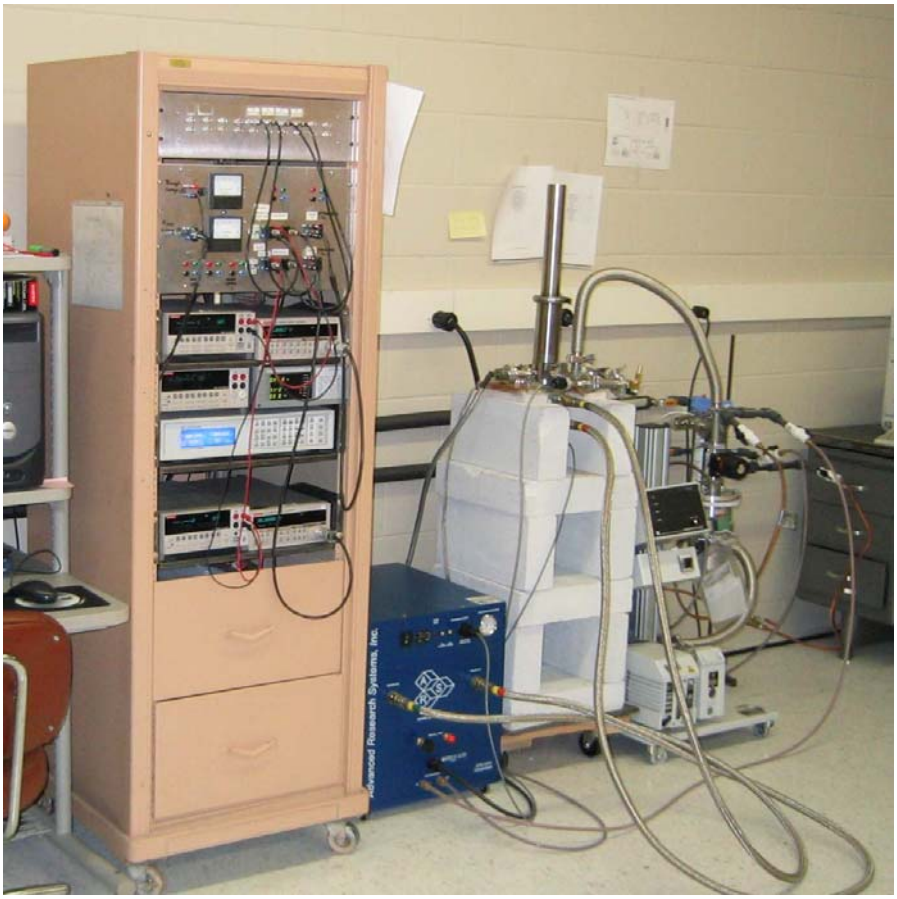

Figure 2.10 Low thermal conductivity measurement system and equipment[13]

Figure 2.11. ZEM Equipment

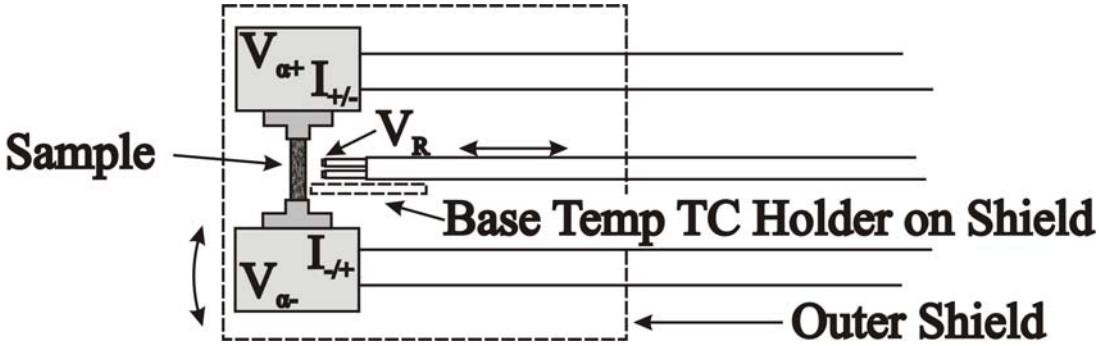

Figure 2.12 High Temp R&S (ULVAC ZEM-2) Probe Head

Source : THE THERMOELECTRIC PROPERTIES INVESTIGATION OF X0.05Mo3Sb7-yTey by Tim C. Holgate

Figure 2.13 Low temperature R&S system[13]

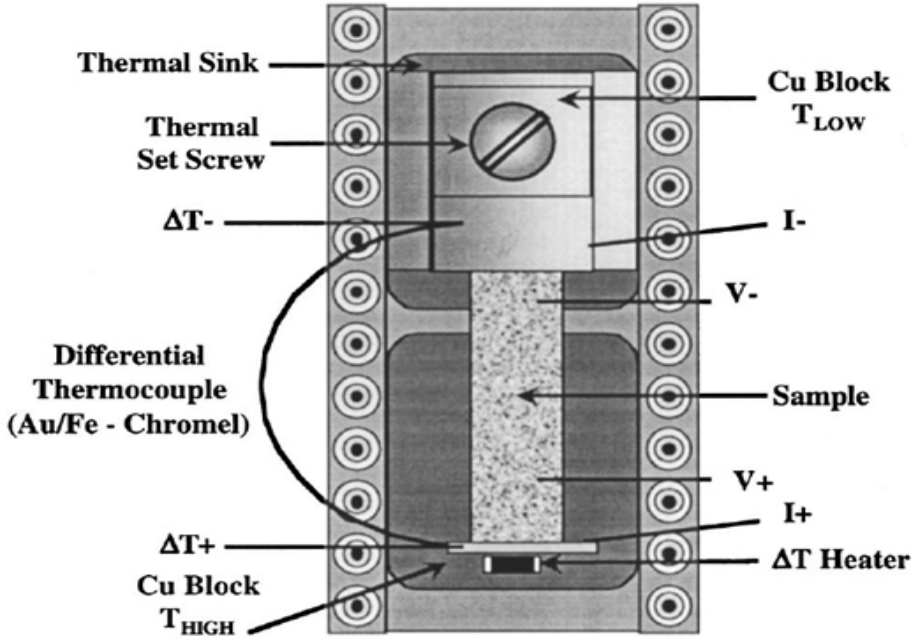

Figure 2.14 Specially designed mounting chip[16]

Figure 2.15 MiniFlex x-ray diffraction system[13]

Figure 2.16 FESEM-Hitachi S4800[17]

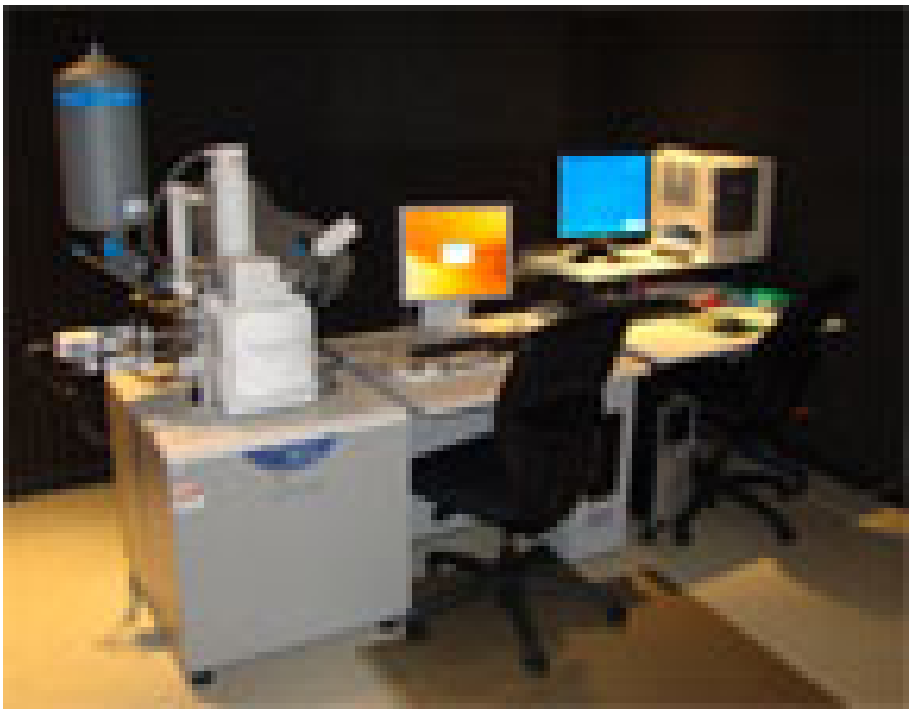

Figure 2.17 SEM3400 S-3400N[17]

CHAPTOR THREE

Results and Discussion

Pb:Te:Ag:Se mixtures series

X-ray Diffraction

Figure 3.1 shows the diffraction patterns for the Pb:Te:Ag:Se mixtures series samples. The black circles were the peak locations of stoichiometric PbTe. It shows a predominantly single phase alloy of the PbTe structure, but with a lattice parameter of α=6.17 A.[11] The reduction in the lattice parameter was due to the size difference between Pb and Ag atoms. In addition, the impurity phase Ag_2Te caused the presenting of extra peaks in the Figure. The impurity concentration was reduced in the $(PbTe)_2(Ag_2Se)_1$ alloy while the lattice parameter of $(PbTe)_2(Ag_2Se)_1$ increased to α= 6.33A. This was a result of doubling the PbTe concentration. The lattice parameter was closer to the value of stoichiometric PbTe when the PbTe concentration was increased.[11]

EDX Data and Phase diagram

It was observed that the mixture of Pb:Te:Ag:Se in a 1:1:2±δ:1 molar ratio gives rise to what appears to be a predominantly single phase alloy.[11] According to the x-ray diffraction data, the dominant phase was in an fcc structure. However, two distinct phases were presented in the EDX analysis (Figure 3.2). One was doped β-Ag_2Te, which was the dominant phase, and the other was doped PbSe. From the Ag-Te phase diagram (Figure 3.3), β-Ag_2Te crystallizes and forms a fcc lattice. In the phase diagram, Ag_2Te went through two structural phase transitions before it melted at 960^0C.[19,20] The α→β transition (monoclinic to fcc) took place at 145 ^{o}C and the β→γ transition (fcc to bcc) took place at 802 ^{o}C.[11]Accordingly, the results

shows that the synthesis of the samples of Pb:Te:Ag:Se in a 1:1:2:1 molar ratio stabilized the high-temperature phase β-Ag_2Te. During the experiment, the samples with small difference in Ag molar ratio (Pb:Te:Ag:Se 1:1:2±x:1) were synthesized to investigate how the ratio affects the properties of the samples. In the x-ray patterns, the samples with 2±x=1.9 showed no difference from the 2.0 samples. However, in the phase diagram, the stable phase β-$Ag_{1.9}Te$ undergoes the transition β-$Ag_{1.9}Te$ → β-Ag_2Te + L at a temperature of 460 ^oC.[11] Also, at temperatures above 460 ^oC, the material lost was observed through SPS synthesis and the measurement of the thermoelectric properties. Therefore, the measurements of the samples were taken below 400 ^oC.

Microscope SEM images

Figure 3.4 shows the SEM image of PbTe-$Ag_{1.9}Se$ SPS at 400 ^oC, Figure 3.5 is the SEM image of PbTe-$Ag_{1.9}Se$ SPS at 500 ^oC, and Figure 3.6 is the SEM image of PbTe-$Ag_{1.9}Se$ melt sample. These three samples have the same molar ratio but incurred different synthesis methods. There are clear differences between the images. In Figure 3.4, numerous small particles and caves are shown in the SPS at 400 ^oC samples. The small particles and caves are clearly shown in SEM images of SPS at 400 ^oC with particle sizes ranging from 3um to 500nm （Figure 3.7-3.8). However, there are less particles and caves in the samples SPS at 500 ^oC and almost no particles and caves in the melt samples. The difference between these three samples can be explained from the phase diagram Figure 3.3. According to the phase diagram, the sample undergoes solid-liquid phase, which gives the material more fluidity and more mobility. The liquid material sits in the caves and the small particles stick together.

Smart mapping and EDX

Smart mapping of these samples is shown in Figure 3.9. In the case of 1.9 ratio samples, it was expected to observe a 2-phase alloy because of the competition between the cubic-PbSe structure and the monoclinic α-Ag2Te structure.[11] Instead, a single phase alloy which forms in a fcc structure was observed. However, from a closer examination of smart mapping and EDX, a 2-phase alloy consisting of fcc-$PbSe_{1-x}Tex$ mixed with room temperature stabilized fcc-β-$Ag2Te_{1-x}Se_x$ with the same lattice parameter was found.[11] In the smart map, Se is shown in green dots, Ag is shown in red dots, Te is shown in yellow dots and Pb is shown in blue dots. Noticeable, the red dots follow the same path as the green, and the blue are similar as the yellow. In conclusion, Ag congregated close to Te in the samples, rather than Se.

The EDX of the PbTe-Ag1.9Se SPS at 400 ^{o}C sample is shown in Figure 3.10 and Figure 3.11. In Figure 3.10, there were Ag and Te in the pink square region at atomic ratio around 1.9:1, but there was no presence of Pb and Se. Figure 3.11 showed the atomic ratio of the bright small particles. Therefore, the Ag_2Te became a dominate phase with PbSeTe doped inside.

Electrical Transport Properties

Figure 3.12 shows the resistivity versus temperature for sample series (PbTe)(AgxSe). The red dots were x=1.9 and directly measured from the melt sample after it was taken out of the furnace. The purple dots were from the sample with x=1.9 and SPS at 400 ^{o}C and the brown dots were from the sample with x=1.9 and SPS at 500 ^{o}C, both occurring after ball-milling of the melt sample. The green, blue and black dots were from x=2, 2.01,2.02, respectively. There was a phase transition around 425 K in all of the samples, except the x=1.9 melt sample. There were no other obvious phase transitions found.

Figure 3.13 shows the temperature dependence of the power factor, $\alpha^2\sigma T$, for the samples. The samples with x=1.9 shows an increasing trend at higher measured temperatures. However, the oncoming β-$Ag_{1.9}Te \rightarrow \beta$-$Ag_2Te$ + L phase transition at 460 ^oC creates an upper limit to the power factor.[11]

Figure 3.14 shows the temperature dependence of the thermal conductivity. The thermal conductivity of the x=1.9 melt sample was very low. The structural disorder gives rise to a much reduced thermal conductivity when compared to stoichiomitric Ag_2Te. Specifically, the total thermal conductivity for all samples measured with x=1.9 melt was $\kappa_T < 0.6$ W/m-K at 575K.[11] Meanwhile, the thermal conductivity data is persistent and does not vary from sample to sample.

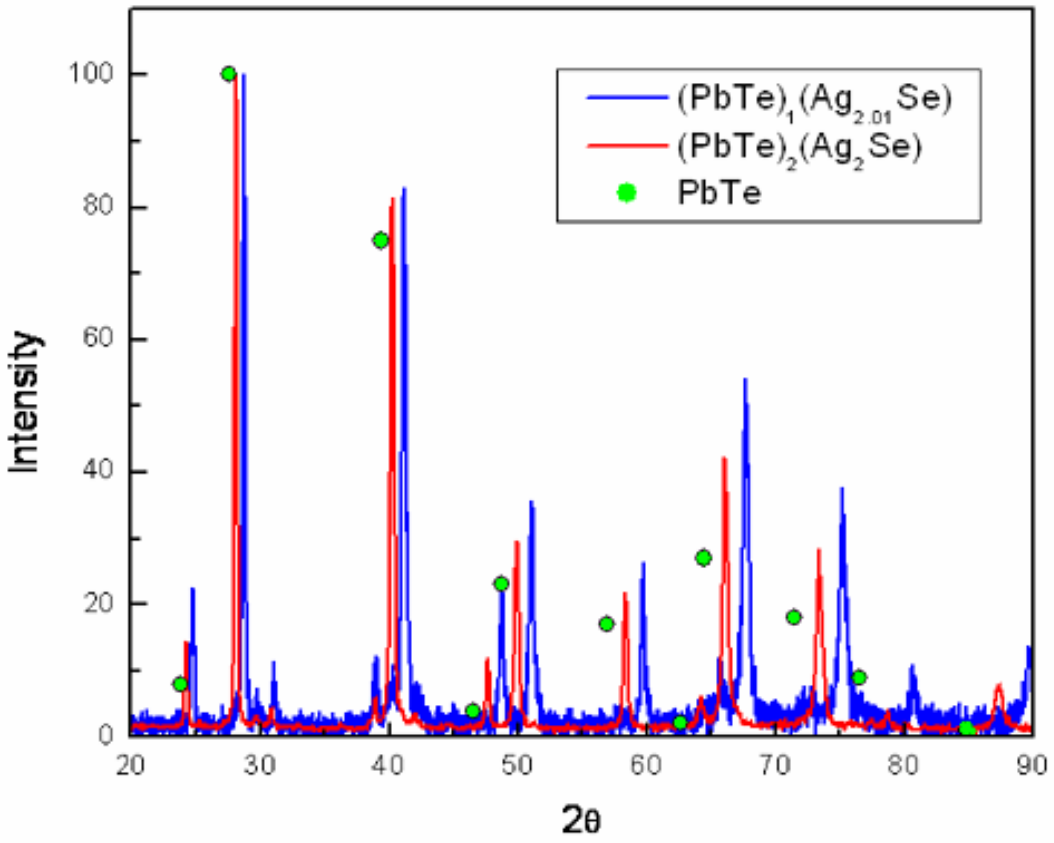

Figure 3.1 X-ray diffraction patterns

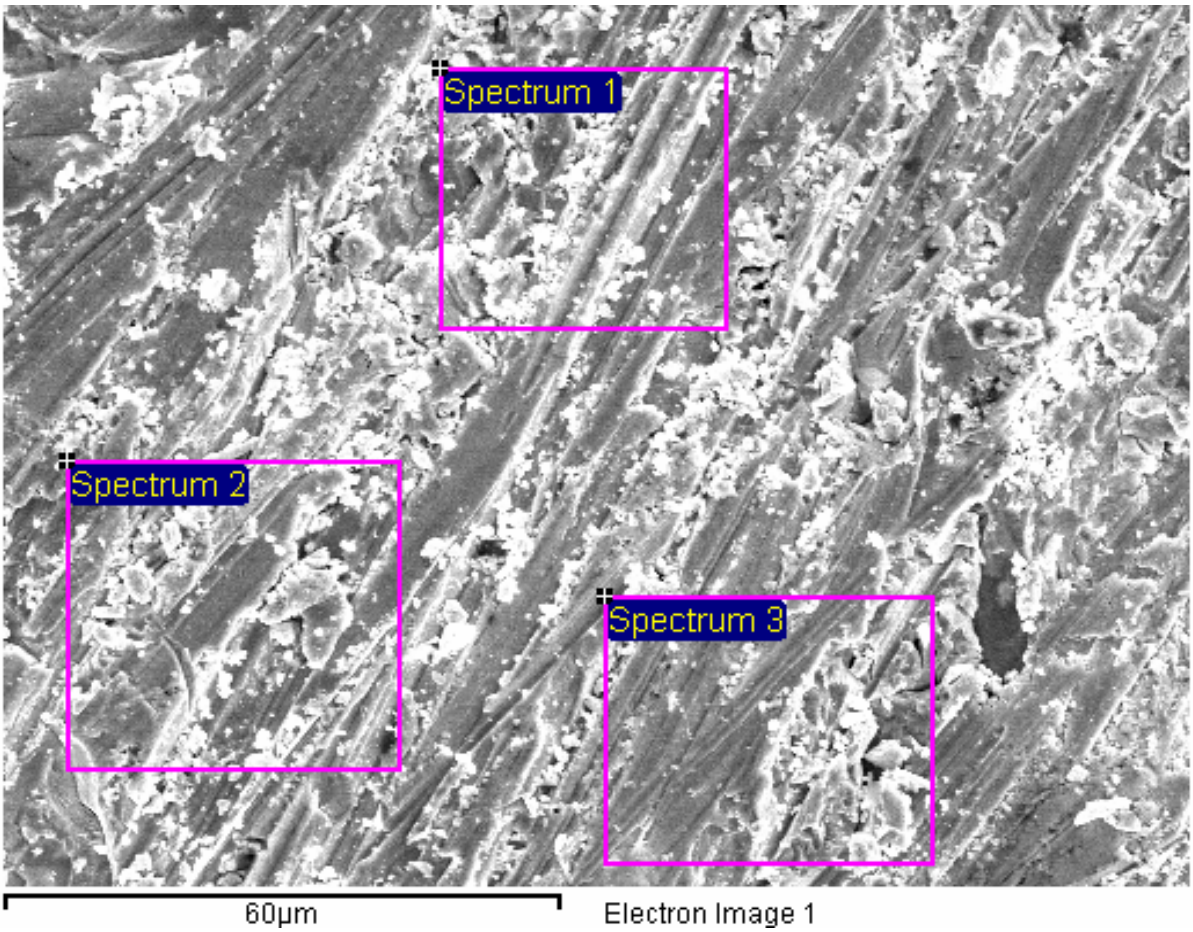

Spectrum	Se	Ag	Te	Pb	Total
Spectrum 1	8.02	50.12	28.22	13.64	100.00
Spectrum 2	10.88	45.67	24.61	18.84	100.00
Spectrum 3	4.18	57.87	30.69	7.26	100.00

Figure 3.2 EXD

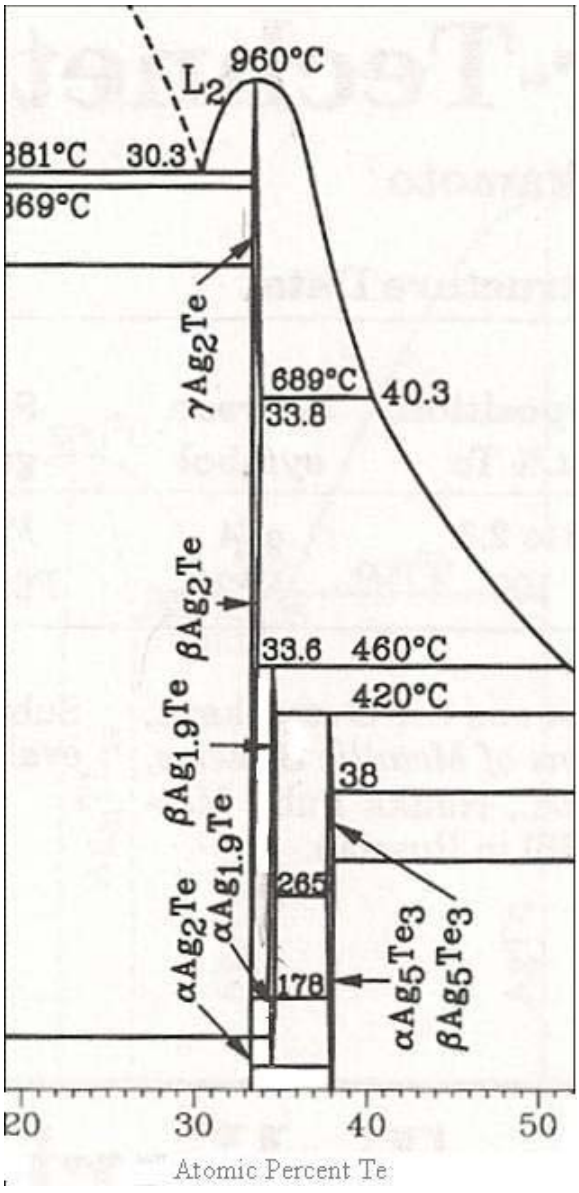

Figure 3.3 Phase Diagram of Ag-Te

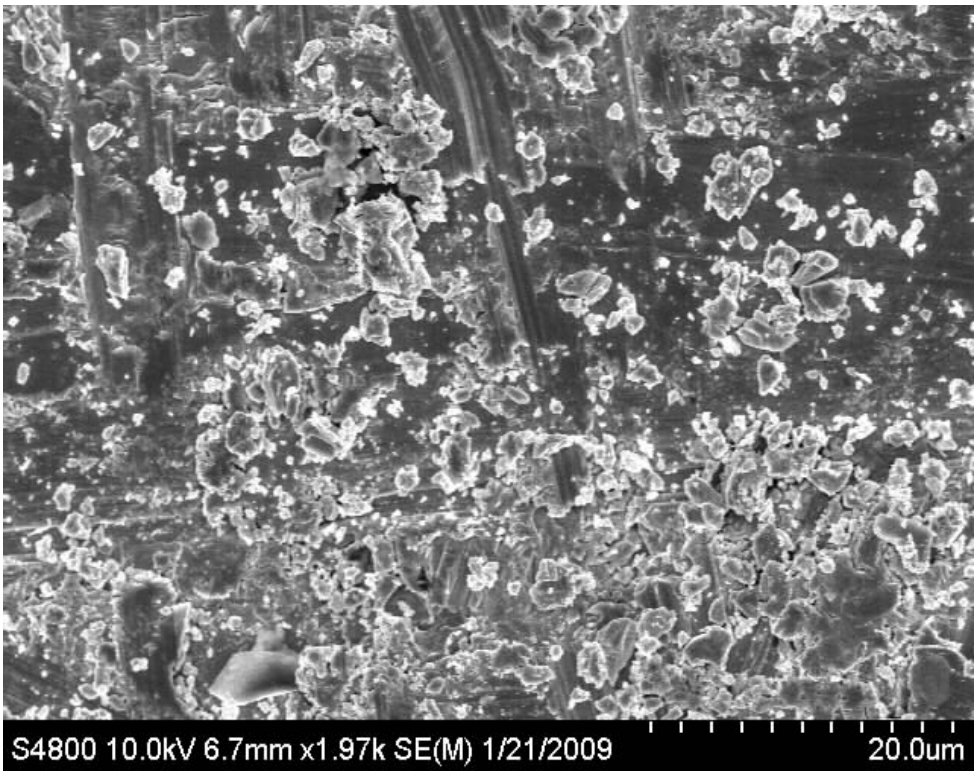

Figure 3.4 SEM image of PbTe-Ag1.9Se SPS at 400 ^{o}C

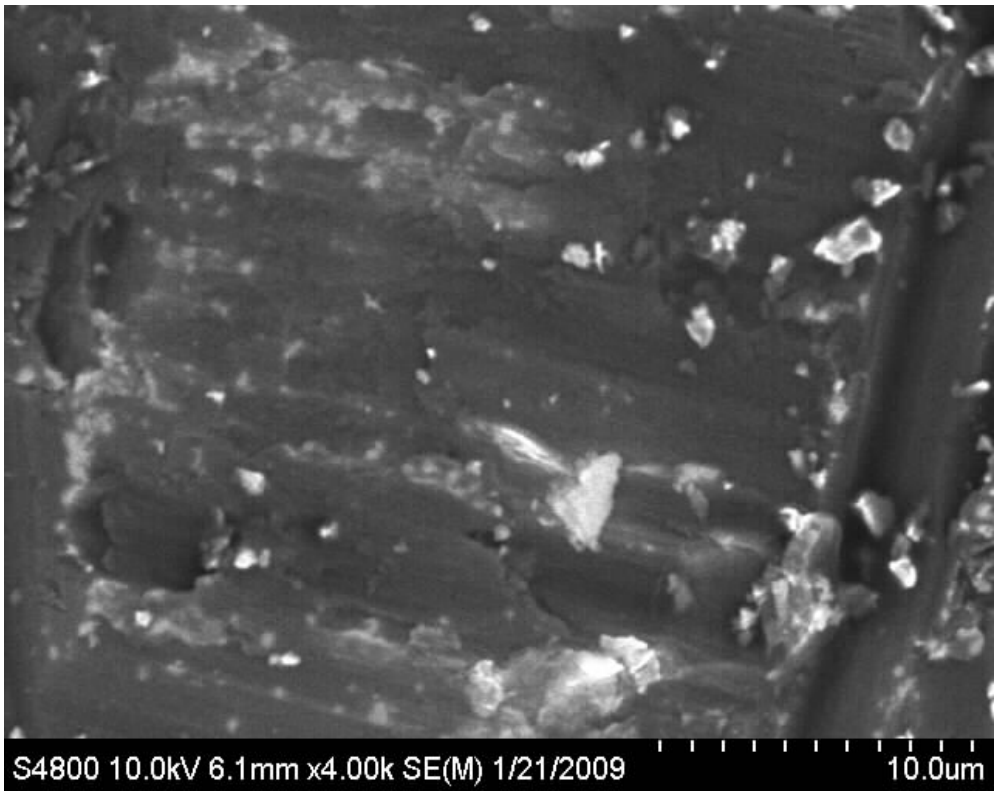

Figure 3.5 SEM image of PbTe-Ag1.9Se SPS at 500 ^{o}C

Figure 3.6 SEM image of PbTe-Ag1.9Se Melt

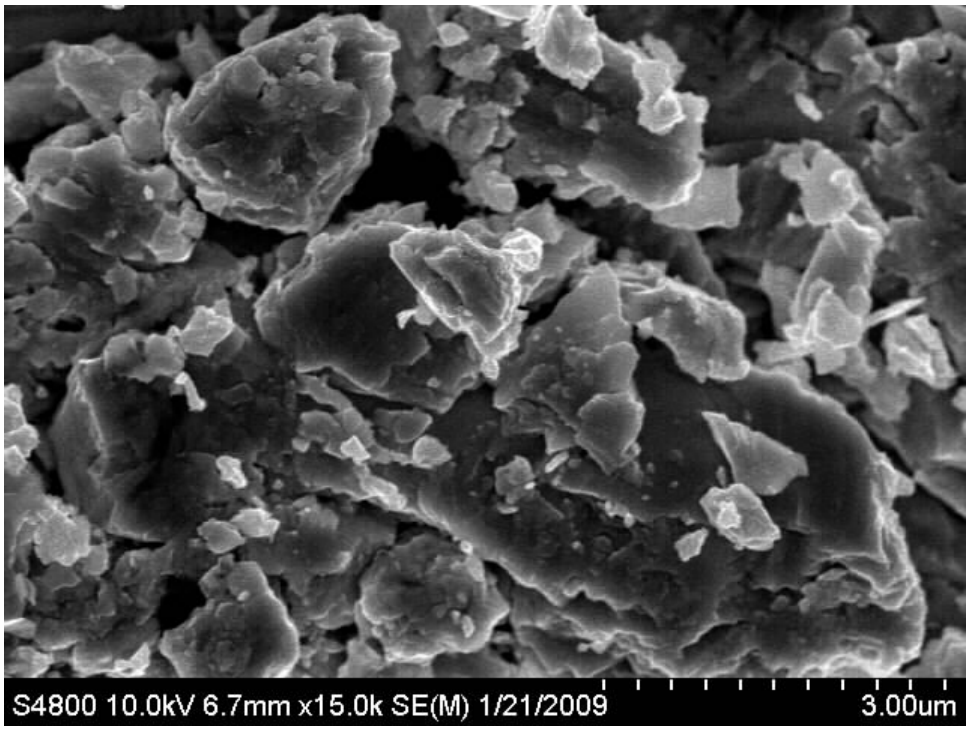

Figure 3.7 SEM image of PbTe-Ag1.9Se SPS at 400 ^{o}C in 3um

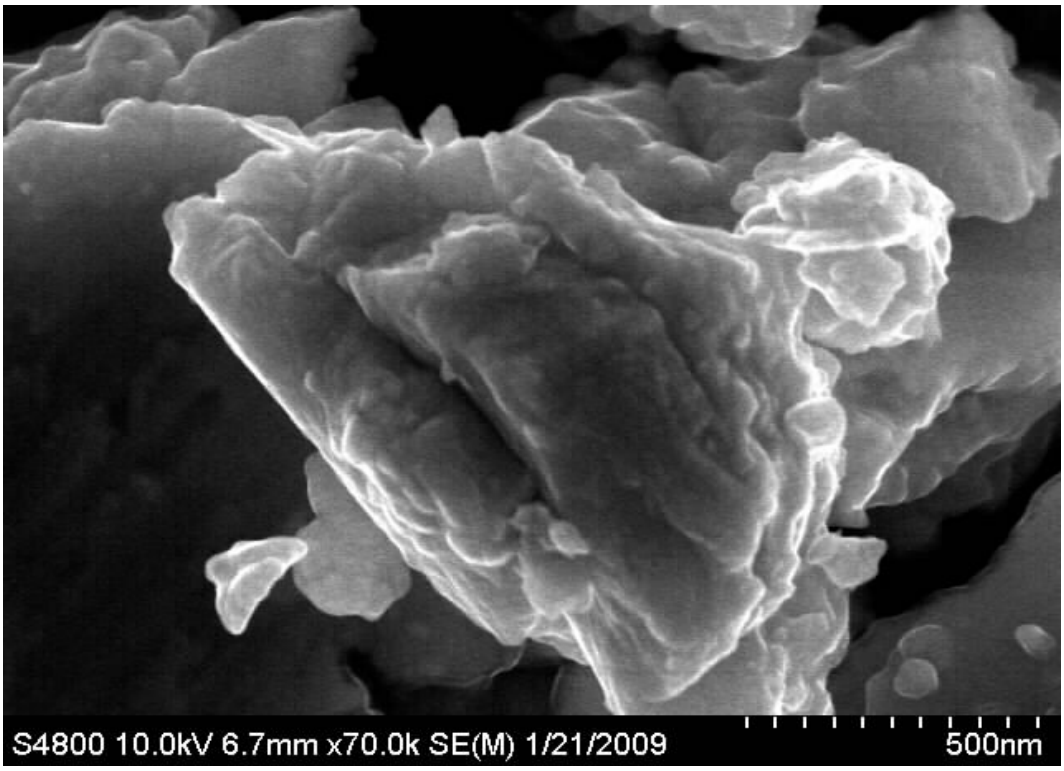

Figure 3.8 SEM image of PbTe-Ag1.9Se SPS at 400 ^{o}C in500nm

Electron Image 1

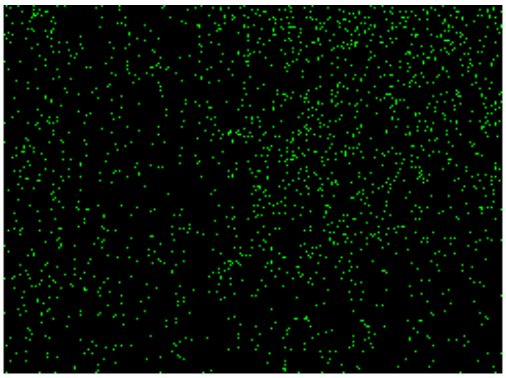

Se Ka1

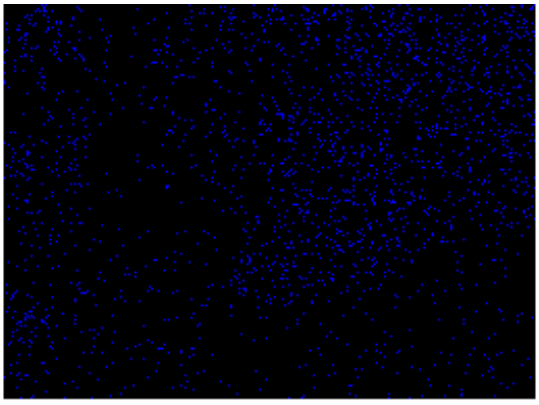

Pb La1

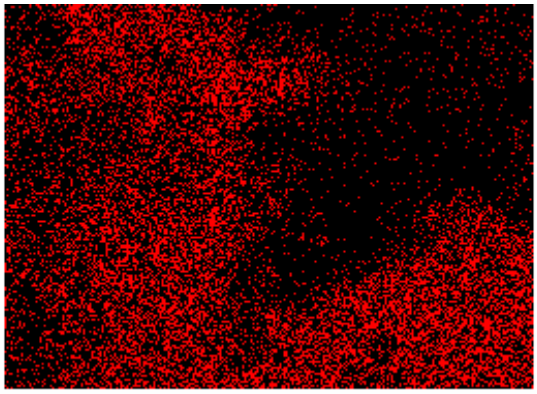

Ag La1

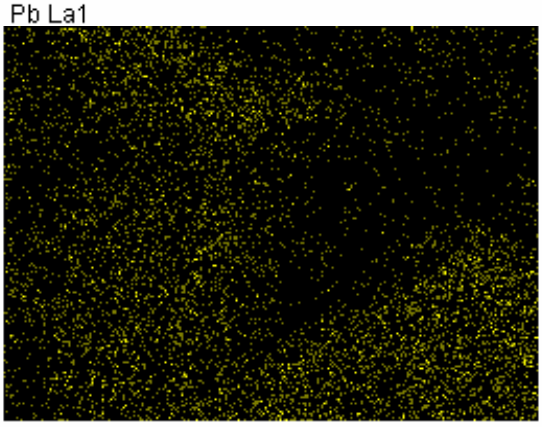

Te La1

Figure 3.9 Smart mapping of PbTe-Ag1.9Se SPS at 400 ^{o}C

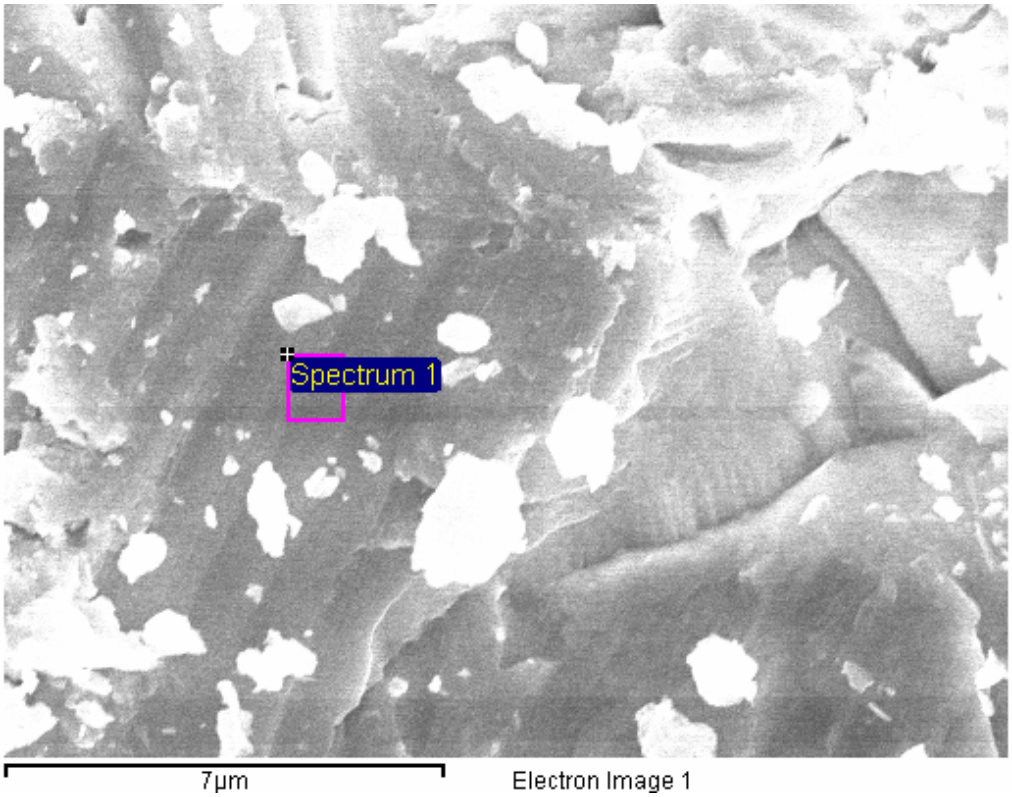

Element	Weight%	Atomic%
Ag L	60.89	64.81
Te L	39.11	35.19

Figure 3.10 EDX of PbTe-Ag1.9Se SPS at 400 ^{o}C

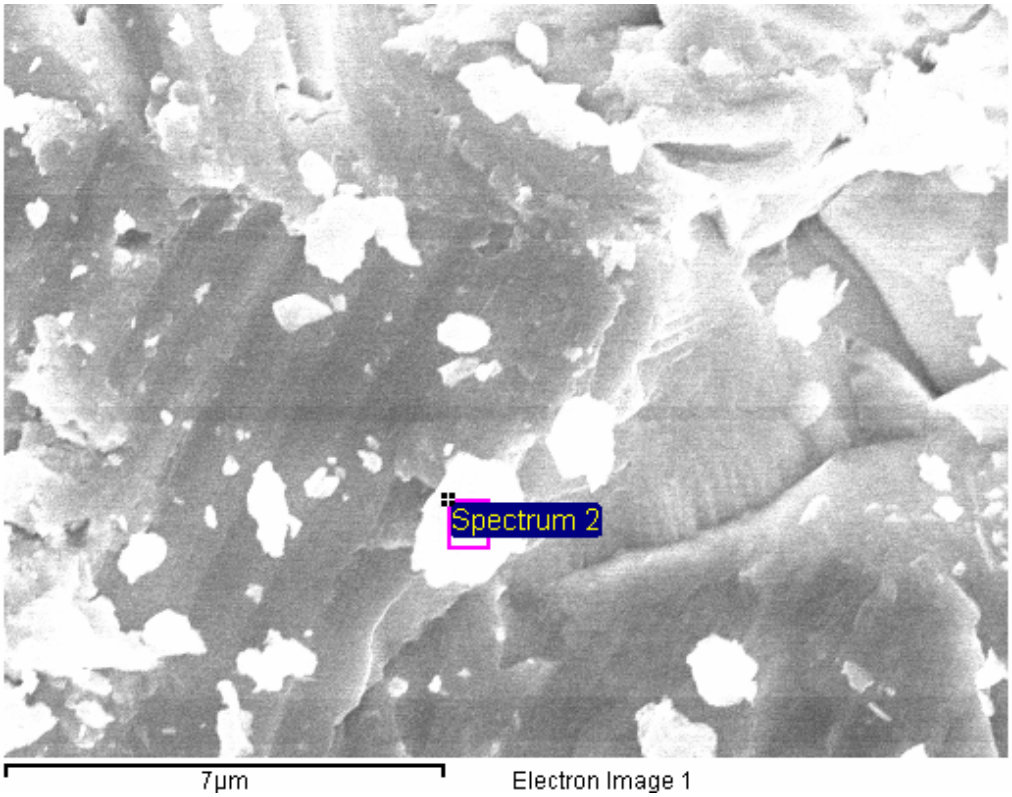

Element	Weight%	Atomic%
Se L	21.24	35.63
Ag L	15.71	19.29
Te L	11.95	12.40
Pb M	51.11	32.68

Figure 3.11 EDX of PbTe-Ag1.9Se SPS at 400 ^{o}C bright particles

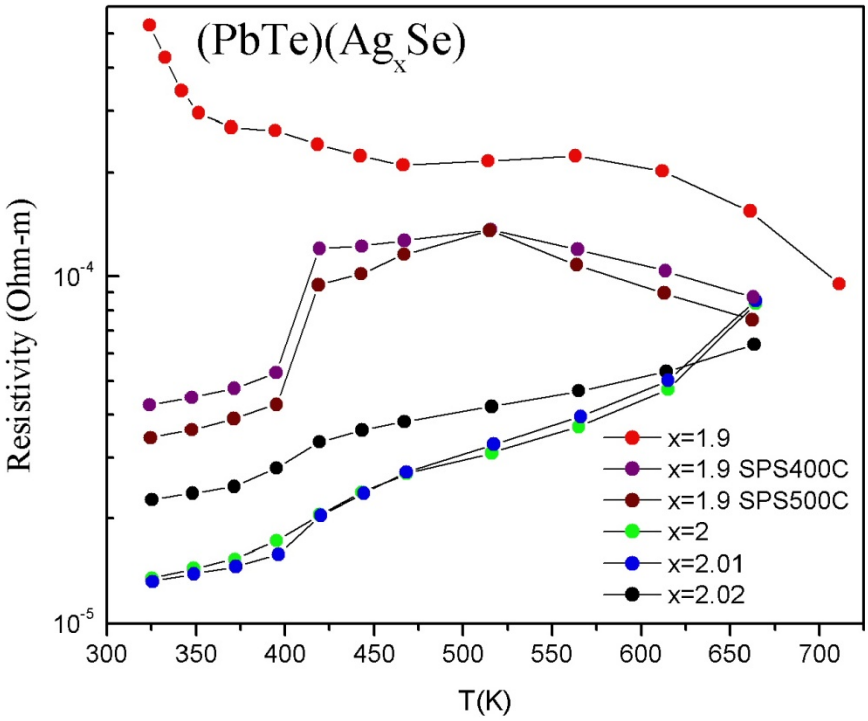

Figure 3.12 Resistivity versus Temperature

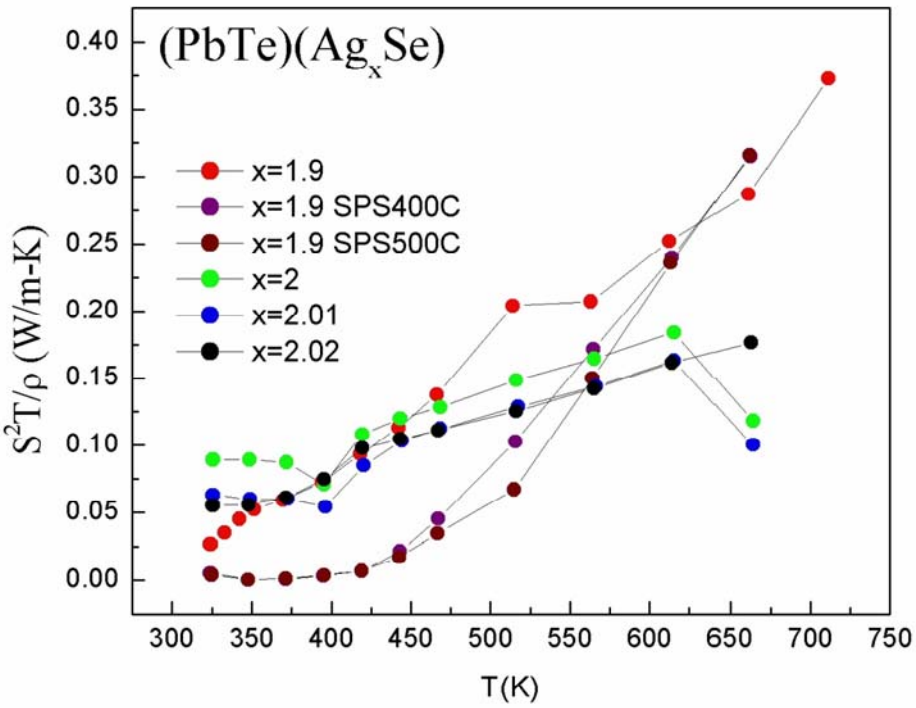

Figure 3.13 Power factor versus Temperature

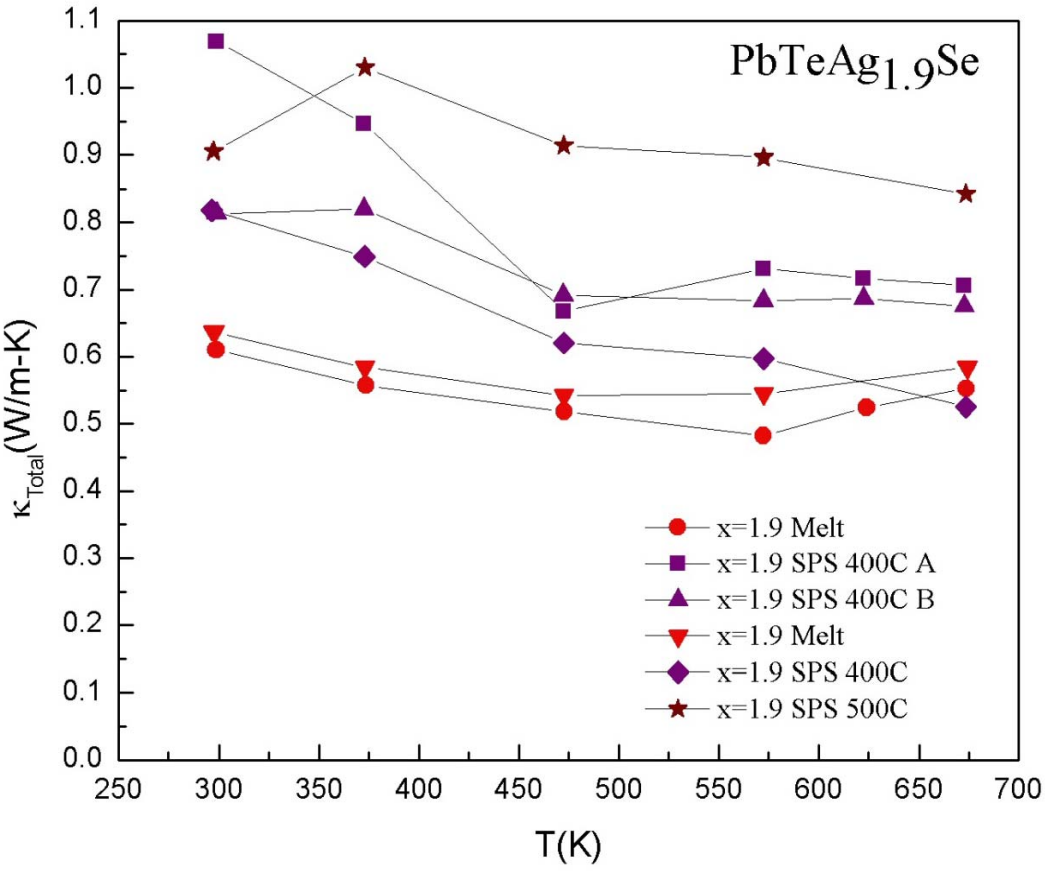

Figure 3.14 Thermal Conductivity versus Temperature

$Cu_xAg_{3-x}SbSeTe_2$

The X-ray diffraction data of $Cu_xAg_{3-x}SbSeTe_2$ samples are shown in Figure 3.15. This figure shows two phases, one crystallizing in the $AgSbTe_2$ rocksalt structure [21] and the other crystallizing in the monoclinic α-Ag_2Te structure [22].[12] The average density of the samples is d=7.30 g/cm^3, which is higher than the density of $AgSbSe_2$ (d=6.69 g/cm^3), slightly higher than the density of $AgSbTe_2$ (d=7.12 g/cm^3) and significantly lower than the density of α-Ag_2Te (d=8.21 g/cm^3).

In Figure 3.15, the X-ray shows that the lattice parameter for the rocksalt phase is a ~ 5.94 A which is between the lattice parameter of $AgSbSe_2$ (a= 5.79 A) and the lattice parameter of $AgSbTe_2$ (a= 6.07 A). Accordingly, the composition of the resulting mixture is Se-doped $AgSbTe_2$ and Se-doped- α-Ag_2Te. Preliminary EDX on two areas of the sample, with distinct features for the best performing Cu-doped sample, confirmed the existence of both Se-doped $AgSbTe_2$ and Se-doped monoclinic Ag_2Te.[27]

The images of the phase are shown in Figure 3.16 and Figure 3.17. As expected, two different phases are uniformly distributed. The phase separation between the rocksalt structure (dark shade) and the monoclinic structure (light shade) is distinct, and micro-fractures, which are likely due to the strain field between two phases, can be seen at the phase boundaries.

The electrical resistivity dependence of temperature, which is typical of an activated process, is shown in Figure 3.18. This behavior was observed at high temperatures, while the room temperature resistivity is dominated by intrinsic effects.[12] In Figure 3.18, the

feature at 400K corresponds to the α→β structural phase transition in the doped Ag_2Te. The resistivity decreases with increasing Cu concentration from a value of 11.8 mOhm-cm for the x=0 sample to 3.3 mOhm-cm for the best δ = 0.2 sample.

The thermopower of the samples are shown in Figure 3.19. The thermopower of the stoichiometirc and Cu-doped samples, contrast to the resistivity, is very robust and does not vary much from sample to sample. In the figure, n-type behavior is shown at low temperature, while p-type behavior is shown at high temperatures, which transition behavior corresponds to the Ag_2Te α→β structural phase transition.[12] It could be observed that Cu doping did not produce significant difference in the thermopower which indicated that Cu doping does not noticeably affect the band structure. The possible reason for the behavior is that the concentration of micor-structures, which varied from sample to sample, had no effect on the thermopower since the band structure remained unchanged.[12] However, the electrical conductivity could be affected by the micro-fractures, which enhanced electronic scattering and increased the electrical resistivity.

The high temperature thermal conductivity versus temperature is shown in Figure 3.20. The thermal conductivity values for all samples are small and increase with temperature increasing. The low temperature thermal conductivity temperature dependence is shown in Figure 3.21, which shows glass-like behavior. It was observed from the X-ray diffraction data that is a crystalline system, so the glass-like behavior is unexpected. According to the data, it is likely that the glass-like behavior was caused by the large level of disorder, which eliminates translational invariance. Consequently, heat was transported through localized vibrations, which led to the greatly reduced lattice

thermal conductivity. The presence of localized vibrations typically gives rise to a $\kappa_{Phonon} \alpha T^2$ dependence of the thermal conductivity at very low temperatures. [12, 28-31] A $\kappa_{Phonon} \alpha T$ dependence has also been observed at low temperatures in quartz[12,32,33] and the bulk-metallic glass[12,34] $Ni_{59.5}Nb_{33.6}Sn_{6.9.}$

The low temperature thermal conductivity of the range from 1.8K to 3.5K is shown in Figure 3.20. A plateau was observed at a temperature around 4K. The appearance of a plateau in the thermal conductivity is a prominent feature of amorphous solids and it is attributed to a rapidly decreasing phonon mean free path with the increasing frequency.[12,35] The thermal conductivity values for both the stoichiometric and Cu-doped samples, are repeatable and do not vary significantly from sample to sample.

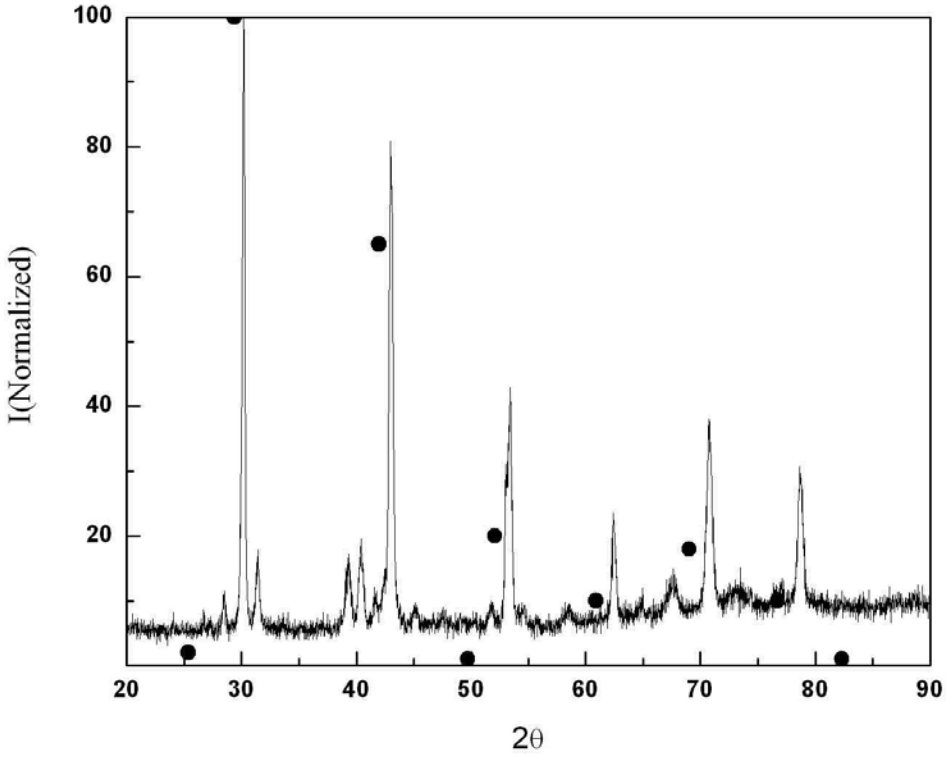

Figure 3.15 X-ray diffraction data of $Cu_{0.2}Ag_{2.8}SbSeTe_2$. The dark circles correspond to the location of the $AgSbTe_2$ peaks

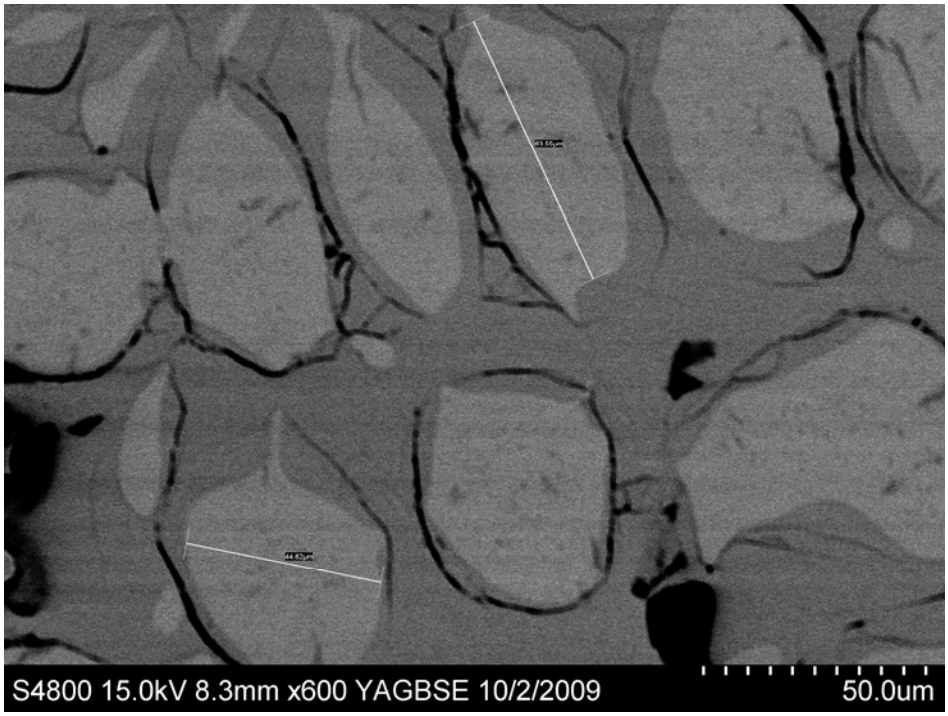

Figure 3.16 SEM image shows the presence of both the cubic AgSbTe2 (dark shade) and monoclinic Ag2Te (light shade). Notice the presence of micro-fractures that exist between the two phases.

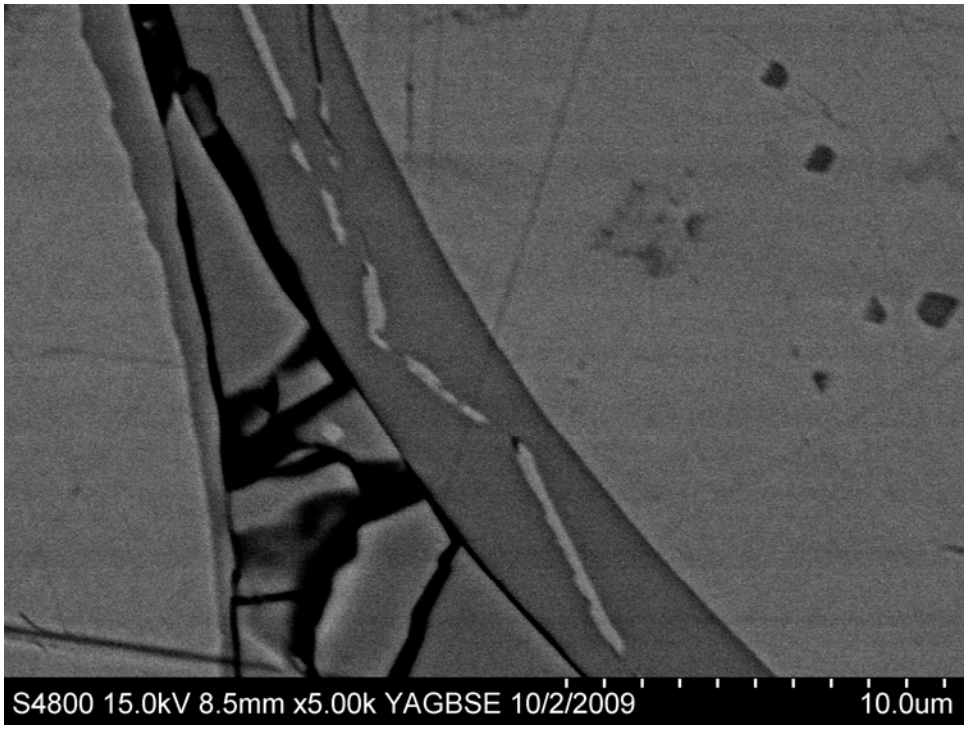

Figure 3.17 Micro-fractures between the different phases

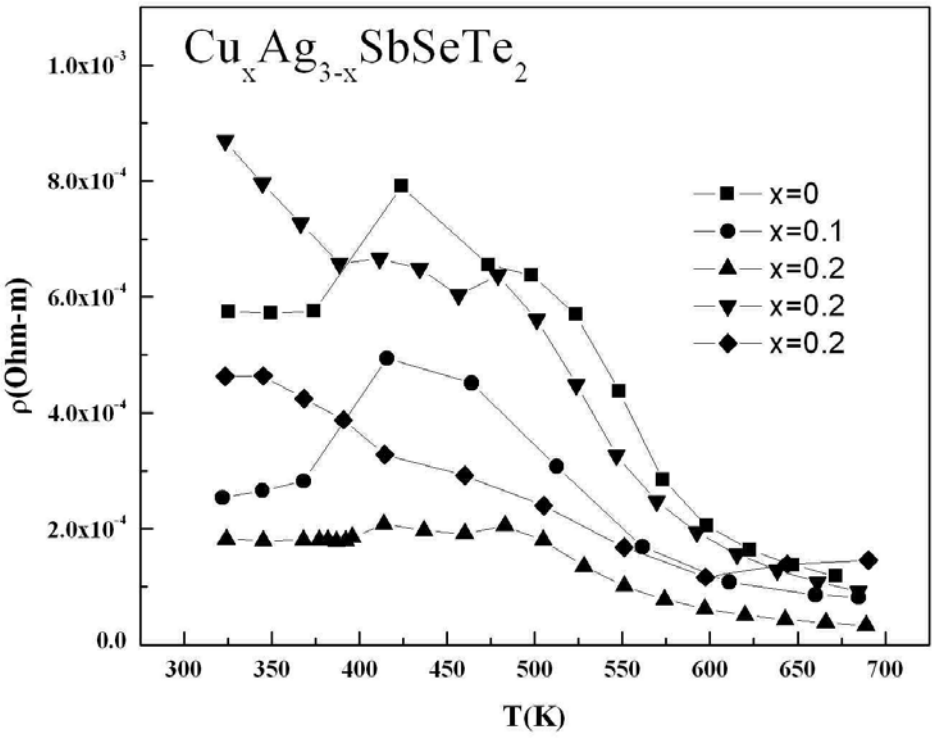

Figure 3.18 Electrical resistivity versus temperature of CuxAg3-xSbSeTe2 for x=0, 0.1 and 0.2.

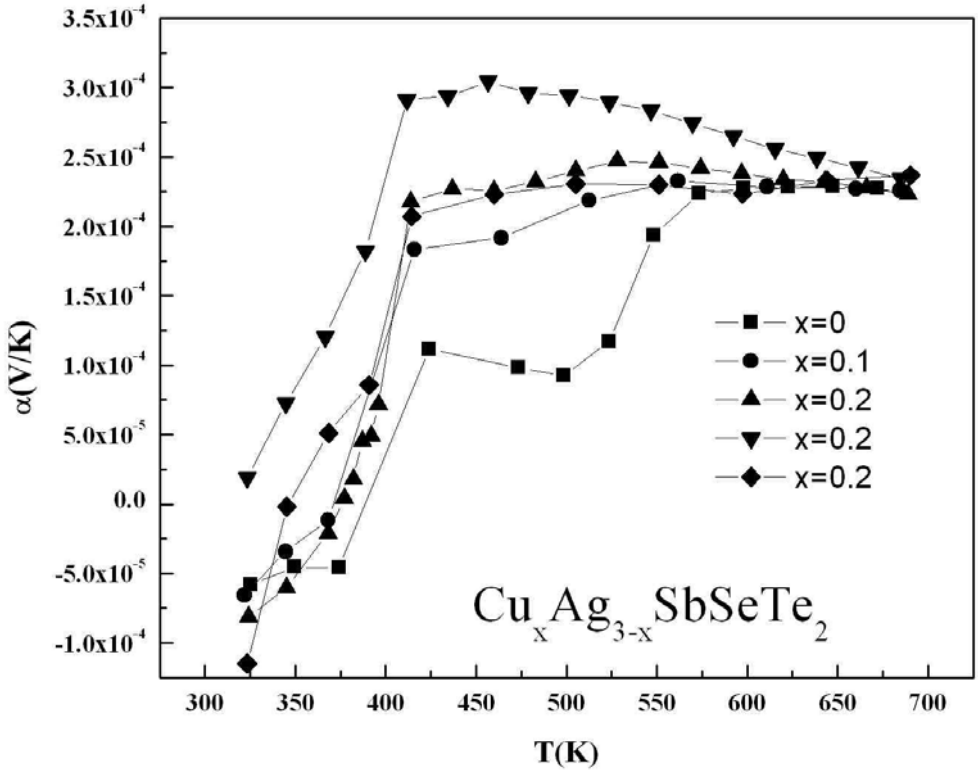

Figure 3.19 Thermopower versus temperature of CuxAg3-xSbSeTe2 for x=0, 0.1 and 0.2

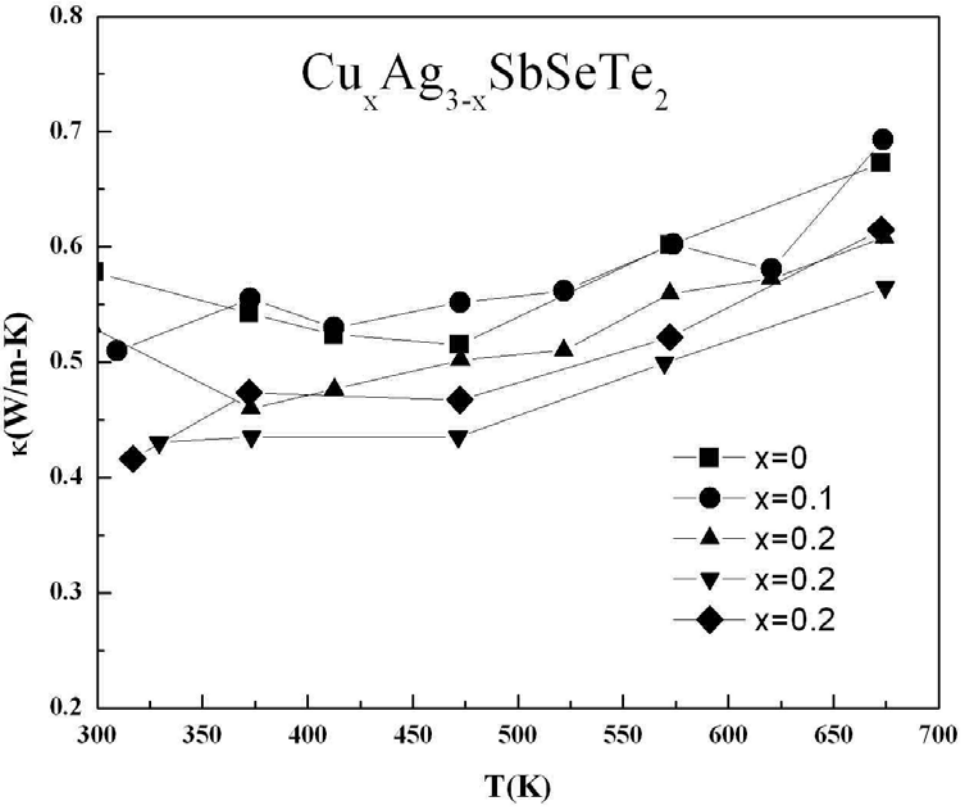

Figure 3.20 High temperature thermal conductivity of CuxAg3-xSbSeTe2 for x=0, 0.1 and 0.2 versus temperature

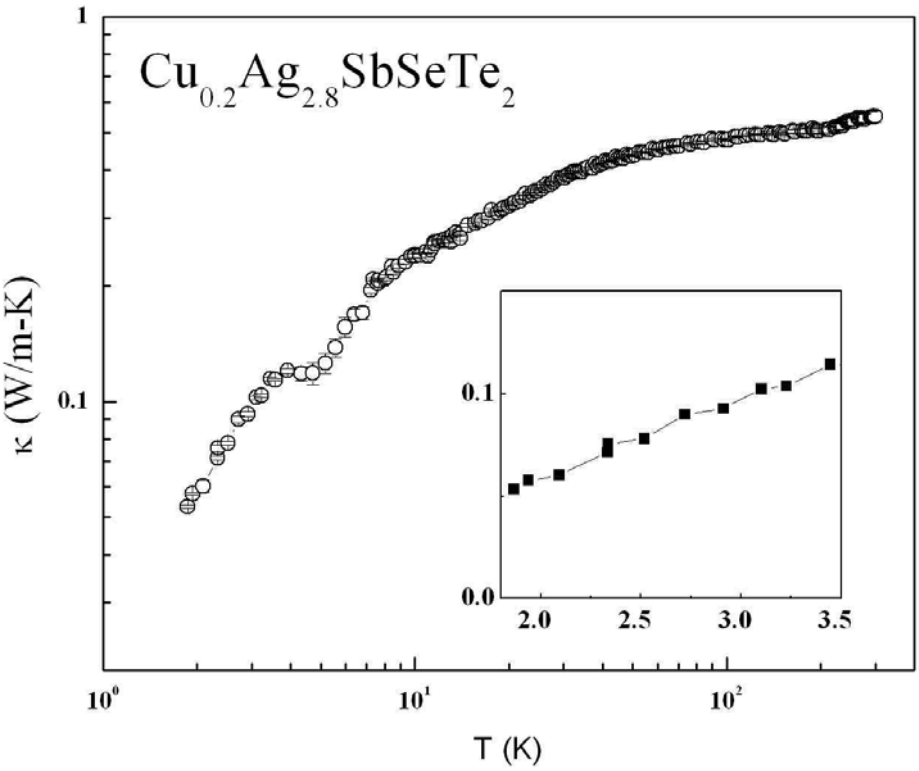

Figure 3.21 Low temperature thermal conductivity Cu0.2Ag2.8SbSeTe2 plotted in log-log scale. The thermal conductivity plateau can be seen at ~ 4 K. The inset (linear scale) shows the linear dependence of the thermal conductivity on temperature

Conclusion

In the Pb:Te:Ag:Se mixtures, EDX examination shows the synthesis of the samples of Pb:Te:Ag:Se in a 1:1:2:1 molar ratio stabilized the high-temperature phase β-Ag_2Te, which is a 2-phase alloy consisting of fcc-PbSe1-xTex mixed with room temperature stabilized fcc-β-$Ag_2Te_{1-x}Se_x$ with the same lattice parameter. The 1: 1:1.9:1 ratio had very low thermal conductivity but a moderate power factor. Therefore, a higher ZT value would be achieved by improvement in the thermopower and electrical conductivity. The mechanical properties of the alloy are significantly improved compared to the PbTe and LAST. The samples are easy to cut, polish and mount for measurement purposes.

The thermal conductivity of x=1.9 melt samples are very low. The structural disorder gives rise to a much reduced thermal conductivity, when compared to stoichiomitric Ag_2Te. Specifically, the total thermal conductivity for all samples measured with x=1.9 melt was $\kappa T < 0.6$ W/m-K at 575K. Illustrating that the thermal conductivity data is persistent and does not vary from sample to sample

For the 2-phase alloy, the electronic and thermal transport shows that the materials have a good potential for high temperature thermoelectric application. The thermopower and thermal conductivity depend weakly on Cu concentration, whereas the resistivity varies considerably. According to the measurement data, it is possible to get high ZT values if lower values of resistivity are achieved by further control of the microstructure and the micro-fractures. Therefore, it can be concluded that a phonon glass can be manufactured into crystalline multi-phase alloys, which may be a promising direction for materials with high thermoelectric performance.

Appendix

Appendix A

Structure formation and very low thermal conductivity in dense Pb:Te:Ag:Se mixtures

(Accepted for publication in Journal of Applied Physics)

Fivos R Drymiotis, Tyler B Drye, Yisha Wang, Jian He, Daniel Rhoades, Kimberly Modic, Samantha Cawthorne, Terry Tritt.

Clemson University, Department of Physics and Astronomy, Clemson SC 29634

Sustainable energy research is currently on the forefront of scientific exploration. Global economic instability and the destruction of the environment because of the use of fossil-fuels for power generation, has led us to reconsider our energy-producing methods. Energy conservation and the development of new energy production techniques are both crucial in order to indefinitely sustain our existence. Thermoelectric materials can play a significant part both in energy conservation and energy production since they can convert wasted heat to useful electrical energy[1-3]. Any heat source, either man made or natural can play the part of the hot-temperature reservoir. For example in automotive applications, thermoelectrics can be used to collect the wasted heat from the exhaust and return it to the vehicle in order to power electrical components, thus removing engine load and decreasing consumption. Alternatively, hot-springs may be used to generate electrical power since they provide a natural temperature reservoir.

For power generation applications, the dimensionless figure of merit ZT (defined as $\alpha^2\sigma T/\kappa$ where α is the thermopower or Seebeck coefficient, σ is the electrical conductivity and κ is the thermal conductivity) must have its maximum value at

temperatures preferably above 600 ^{o}C. Although materials do exist that have a large power-factor (defined as $\alpha^2\sigma T$), their thermoelectric performance is limited due to a large thermal conductivity. The solid-solution technique though has yielded very promising results as far as reducing thermal conductivity. In the case of $(PbTe)_m$-$AgSbTe_2$, presence of nano-scale inhomogeneities led to a significant reduction in the thermal conductivity and a significant improvement of the thermoelectric figure-of-merit with respect to the stoichiometric PbTe[4-6].

We decided to follow a similar approach, but in addition react elements which do not form isostructural lattices. We decided thus to react Pb:Te:Ag:Se in the molar ratio (1:1:1.9:1) in an attempt to monitor the effects of phase competition between the cubic PbSe and the monoclinic Ag_2Te[7-9]. We have observed that the mixture forms what appears to be a predominantly single phase alloy which crystallizes in an fcc structure and has very low thermal conductivity. The lowest thermal conductivity values and the best thermoelectric performance are observed in the p-type Pb:Te:Ag:Se (1:1:1.9:1).

Experimental Section:

Pb, Te, Ag and Se with respective purities of 99.9999%, 99.9999%, 99.9999% and 99.999% were placed in quartz tubes in stoichiometric ratios 1:1:x:1, with x= 1.9, 2.0, 2.01 and 2.02. For the purpose of this letter we will only be discussing the x=1.9 samples since they showed the most promising thermoelectric behavior. The quartz tubes were then evacuated, sealed, and placed inside a box furnace. The samples were subsequently heated to 1000 ^{o}C were they were allowed to remain for 4 hours, before finally allowed to cool down to 500 ^{o}C at a rate of 10^{o}C/hour, at which point the power to the furnace was

turned off. The formed ingots were then removed from the quartz tubes and processed for measurement. The mass of each ingot was approximately 20 grams. All samples obtained were highly dense with good mechanical properties. The density of all samples was approximately 8.05 gr/cm^3 which is greater than the theoretical density of Ag_2Te (7.96 gr/cm^3) but less than the theoretical density of PbSe (8.25 gr/cm^3).

The x-ray diffraction data was obtained using a commercial Rigaku® diffractometer and the SEM and EDX analysis were performed using the Hitachi S3400-N SEM. The high-temperature resistivity and thermopower data were obtained using the ULVAC-ZEM2® measuring system. The high-temperature thermal-conductivity values were deduced from the thermal diffusivity values obtained using the Netzsch LFA 457® laser flash apparatus using the relation $\kappa=\alpha\rho C_V$, with α being the measured value of the thermal diffusivity, ρ the density and C_V the heat capacity at constant volume. The value of ρ used in the calculations was the measured density at room temperature, and the value of C_V was taken to be the value of the DuLong Petit limit.

Results and Discussion

We have observed that the mixture of Pb:Te:Ag:Se in a 1:1:2±δ:1 molar ratio, gives rise to what appears to be a predominantly single phase alloy. The dominant phase, according to the x-ray diffraction data, crystallizes in an fcc structure. EDX analysis though, shows the presence of 2 distinct phases, doped β-Ag_2Te (dominant) and doped-PbSe, with the β-Ag_2Te phase being noticeably more abundant. The x-ray analysis and the transport data also confirm the existence of small traces of another phase, presumably the monoclinic α-Ag_2Te. According to the Ag-Te phase diagram[10, 11], only β-Ag_2Te

crystallizes in an fcc lattice. Ag_2Te undergoes 2 structural phase transitions before it melts at 960 ^oC (figure 1). The $\alpha \rightarrow \beta$ transition (monoclinic to fcc) takes place at 145 ^oC and the $\beta \rightarrow \gamma$ transition (fcc to bcc) takes place at 802 ^oC. Our results indicate that reacting Pb:Te:Ag:Se in a 1:1:2:1 molar ratio stabilizes the high-temperature phase β-Ag_2Te. However, if the mixture is off-stoichiometry i.e. Pb:Te:Ag:Se 1:1:1.9:1, the stable phase is β-$Ag_{1.9}Te$, which undergoes the transition β-$Ag_{1.9}Te \rightarrow$ β-Ag_2Te + L at a temperature of 460 ^oC. No difference was observed in the x-ray patterns of the x=1.9 and x=2.0 samples. We have observed deterioration of the x = 1.9 samples for temperatures > 460 ^oC indicating that the sample is indeed going through the β-$Ag_{1.9}Te \rightarrow$ β-Ag_2Te + L transition. All our measurements are therefore taken below 400 ^oC. The relevant part of the Ag-Te phase diagram is shown in figure 1.

The most astounding result, though, concerns the lattice parameter of the dominant phase β-Ag_2Te. According to the ICDD database, the lattice parameter of β-Ag_2Te is 6.585 A but the lattice parameter we obtained from the x-ray diffraction patterns is 6.157 A - which is much closer in value to the lattice parameter of PbSe (6.130 A). The EDX data confirms the existence of both β-Ag_2Te and doped-PbSe but the x-ray diffraction data though shows peaks corresponding to essentially a single fcc phase (figure 2). In order for this x-ray diffraction scenario to be possible, doped-β-Ag_2Te and the doped PbSe must have the same lattice parameters. Since the mixture was heated only up to 1000 ^oC, and the melting point of PbSe is 1079 ^oC, the mixture at 1000 ^oC most probably contained solid Ag- and Te-doped PbSe in equilibrium with liquid Ag and Te. As the mixture was cooled below 1000 ^oC, the presence of the fcc doped-PbSe forced Ag and Te

to solidify in the fcc β-Ag_2Te structure but with a much reduced lattice parameter. In order to confirm our findings, we synthesized several samples of Pb:Te:Ag:Se in a 1:1:1.9:1 molar ratio and repeated the EDX (figure 3) and x-ray diffraction measurements. All samples shared the same structural characteristics so the results are reproducible. In addition, we did not observe changes in the structure after the samples were heated to 400 ^oC, which implies that the structural arrangement is robust. Deterioration of the structure was only observed for samples heated > 460 ^oC, due to the β-$Ag_{1.9}Te \rightarrow$ β-Ag_2Te + L phase transition. In other words, the behavior of these samples is reproducible and robust up to 400 ^oC.

The structural disorder gives rise to a much reduced thermal conductivity, when compared to stoichiometric Ag_2Te. Specifically, the total thermal conductivity for all samples measured, with stoichiometry 1:1:1.9:1, was $\kappa_T < 0.6$ W/m-K at 675K (figure 4). The thermal conductivity behavior is persistent and does not vary from sample to sample. The resistivity and thermopower values though vary slightly, as expected from degenerate semiconductors, but typical values obtained at 388 ^oC are $\rho \sim 1.6 \times 10^{-4}$ Ohm-m and $\alpha \sim 255 \times 10^{-6}$ V/K. Figure 4 shows the temperature dependence of the power factor, $\alpha^2\sigma T$, for two separate samples. The value of the power factor at 388 ^oC is 0.255 W/m-K for sample A and 0.266 for sample B. Measurements at higher temperatures show an increasing trend but unfortunately the oncoming β-$Ag_{1.9}Te \rightarrow$ β-Ag_2Te + L phase transition at 460 ^oC puts an upper limit to the power-factor. Nonetheless, the maximum ZT value obtained at 661K is ZT = 0.45 which maybe substantially increase at

higher temperature if we are able to stabilize the lattice and improve the electrical conductivity.

The stabilization of an fcc structure, when combining Pb, Te, Ag and Se at a 1:1:1.9:1 molar ratio, is remarkable. Based on our own research on the LAST compounds ($(PbTe)_m$ $AgSbTe_2$), for m=1 we have observed clear phase separation, even though the 2-phases form the same structure and the elements are at a correct molar ratio. In the case of Pb:Te:Ag:Se in a 1:1:1.9:1 ratio, we had expected to observe a 2-phase alloy because of the competition between the cubic-PbSe structure and the monoclinic α-Ag_2Te structure. Instead, we observe what appears to be a single phase alloy which forms in an fcc-structure, but, after closer examination (EDX), it is a 2-phase alloy consisting of fcc-$PbSe_{1-x}Te_x$ mixed with room temperature stabilized fcc-β-$Ag2Te_{1-x}Se_x$ and with both phases having the same lattice parameter. The resulting structure has very low thermal conductivity and although the power factor is moderate, slight improvements in the thermopower and electrical conductivity will result in a higher ZT value. The mechanical properties of the alloy are excellent – the alloy is very easy to cut and polish and does not suffer from the brittleness of PbTe and LAST. Our results, more importantly, indicate that solid mixtures containing elements in ratios forming non-isostructural compounds bear further investigation as a means to reduce thermal-conductivity. We would like to thank DOE-EPSCOR for support of this project.

References

[1] T. M. Tritt, *Thermoelectric materials 2000--the next generation materials for small-scale refrigeration and power generation applications : symposium held April 24-27, 2000, San Francisco, California, U.S.A* (Materials Research Society, Warrendale, Pa., 2001), p. 1 v. (various pagings).

[2] G. S. Nolas, and Materials Research Society. Meeting, *Thermoelectric materials 2003--research and applications : symposium held December 1-3, 2003, Boston, Massachusetts, U.S.A* (Materials Research Society, Warrendale, Pa., 2004), pp. xiv.
[3] L. E. Bell, Cooling, heating, generating power, and recovering waste heat with thermoelectric systems, Science **321**, 1457 (2008).
[4] K. F. Hsu, S. Loo, F. Guo, W. Chen, J. S. Dyck, C. Uher, T. Hogan, E. K. Polychroniadis, and M. G. Kanatzidis, Cubic AgPbmSbTe2+m: Bulk thermoelectric materials with high figure of merit, Science **303**, 818 (2004).
[5] E. Quarez, K. F. Hsu, R. Pcionek, N. Frangis, E. K. Polychroniadis, and M. G. Kanatzidis, Nanostructuring, compositional fluctuations, and atomic ordering in the thermoelectric materials AgPbmSbTe2+m. The myth of solid solutions, Journal of the American Chemical Society **127**, 9177 (2005).
[6] D. I. Bilc, S. D. Mahanti, and M. G. Kanatzidis, Electronic transport properties of PbTe and AgPbmSbTe2+m systems, Physical Review B **74** (2006).
[7] M. Ferhat, and J. Nagao, Thermoelectric and transport properties of beta-Ag2Se compounds, Journal of Applied Physics **88**, 813 (2000).
[8] M. Fujikane, K. Kurosaki, H. Muta, and S. Yamanaka, Thermoelectric properties of alpha- and beta-Ag2Te, Journal of Alloys and Compounds **393**, 299 (2005).
[9] M. Fujikane, K. Kurosaki, H. Muta, and S. Yamanaka, Electrical properties of alpha- and beta-Ag2Te, Journal of Alloys and Compounds **387**, 297 (2005).
[10] M. Kobayashi, Review on Structural and Dynamic Properties of Silver Chalcogenides, Solid State Ionics **39**, 121 (1990).
[11] T. B. Massalski, H. Okamoto, and ASM International., *Binary alloy phase diagrams* (ASM International, Materials Park, Ohio, 1990), pp. 3 v. (xiv.

Figure Captions

Figure 1. Phase diagram of Ag-Te in the region of stoichiometry 2:1.

Figure 2. Normalized x-ray diffraction pattern of Pb:Te:Ag:Se combined in a 1:1:1.9:1 molar ratio. The dark circles correspond to PbSe peak locations. The very low intensity peaks correspond to the monoclinic α-Ag_2Te. The diffraction pattern does not change after the sample has been heated to 400 ^oC.

Figure 3. SEM image of Pb:Te:Ag:Se. EDX measurements on regions 1, 2 and 3 confirmed the coexistence of Se-doped β-Ag2Te (darker areas) and Ag-and Te-doped PbSe (lighter areas).

Figure 4. Total thermal conductivity and power-factor for 2 separately prepared samples of Pb:Te:Ag:Se - 1:1:1.9:1. The maximum ZT at 661 K was ZT ~ 0.45.

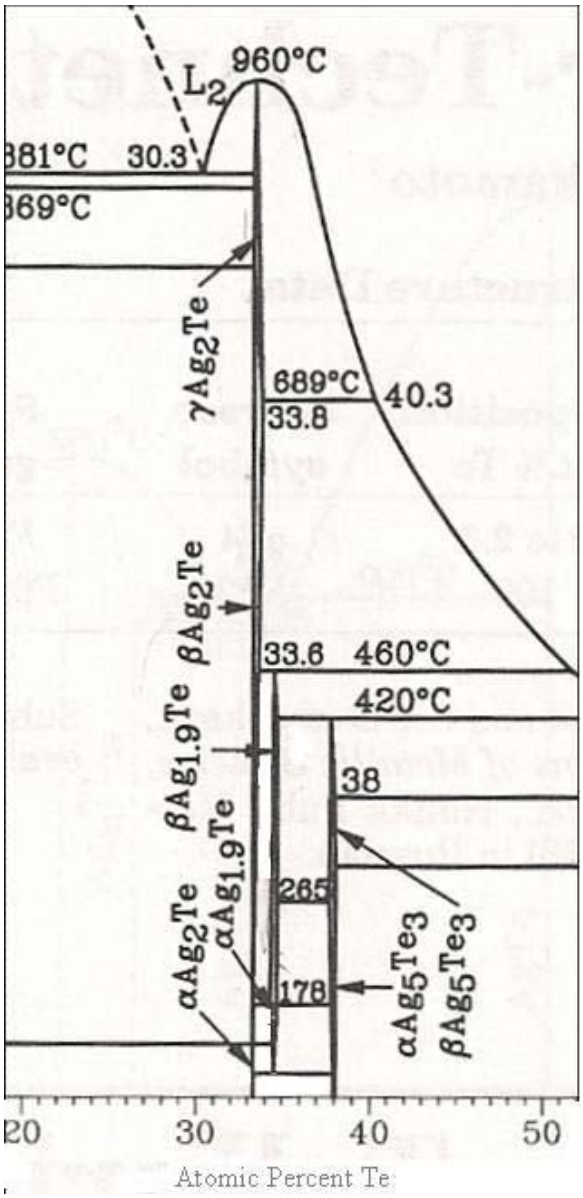
960°C
L2
381°C
30.3
369°C
γAg2Te
689°C
40.3
33.8
βAg2Te
33.6
460°C
420°C
βAg1.9Te
38
αAg1.9Te
αAg2Te
265
178
αAg5Te3
βAg5Te3
20
30
40
50
Atomic Percent Te

Figure 1.

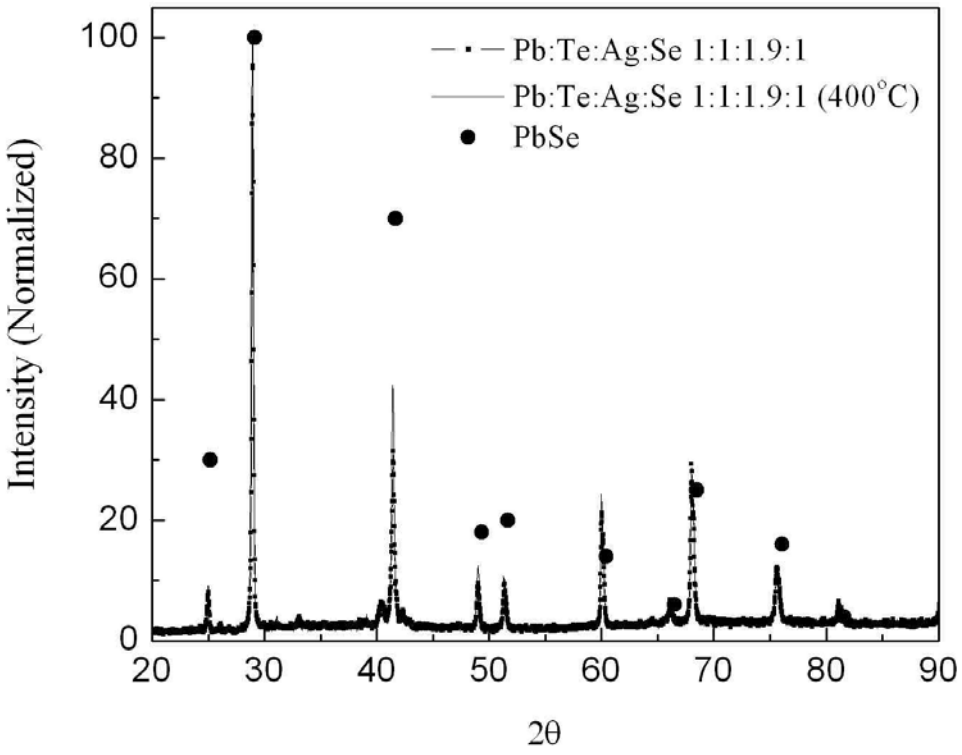
Pb:Te:Ag:Se 1:1:1.9:1
Pb:Te:Ag:Se 1:1:1.9:1 (400°C)
PbSe
Intensity (Normalized)
2θ
0
20
40
60
80
100
20
30
40
50
60
70
80
90

Figure 2.

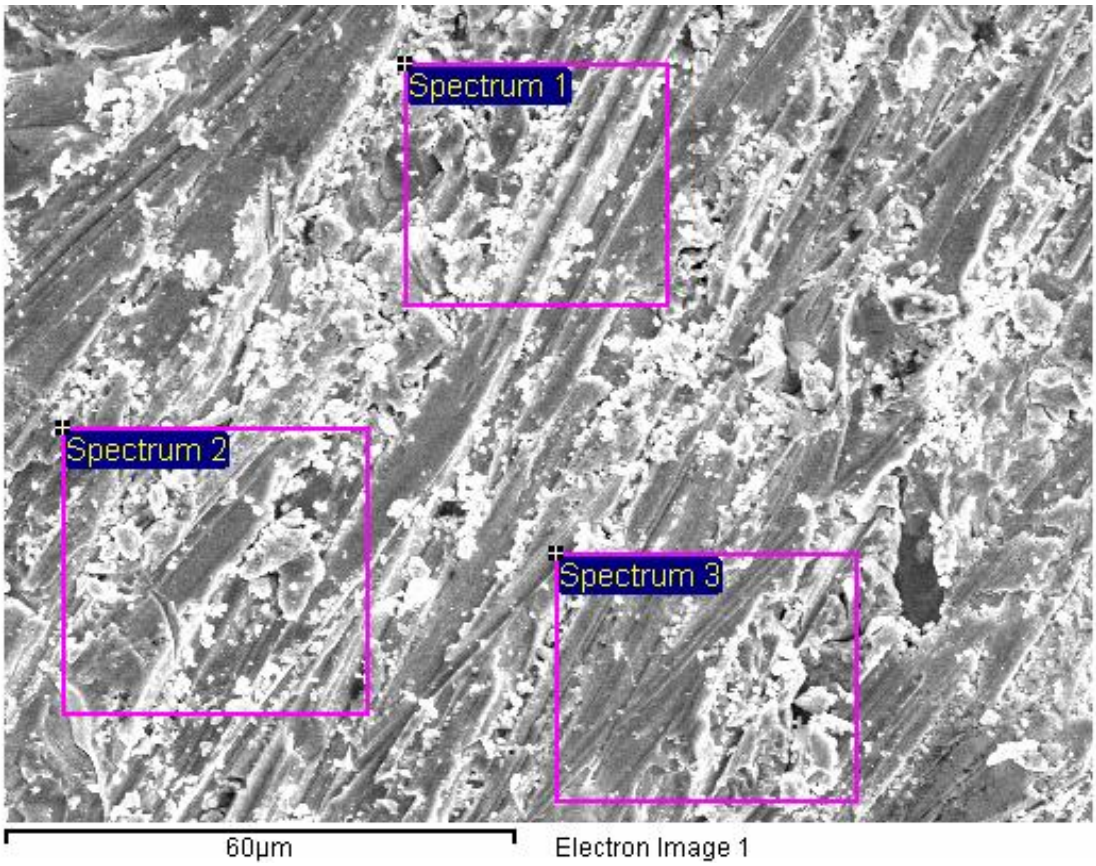

Figure 3.

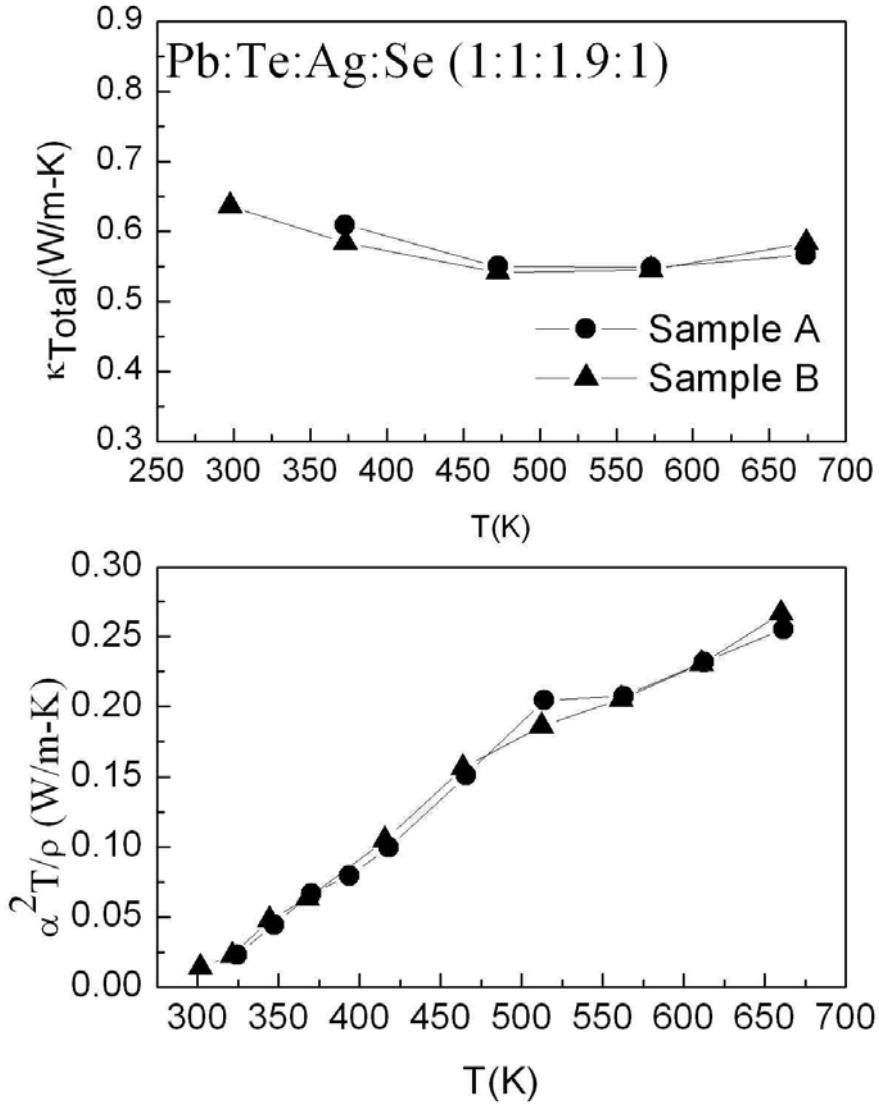

Figure 4.

Appendix B

Glassy Thermal Conductivity in the 2-phase $Cu_xAg_{3-x}SbSeTe_2$ alloy and High-Temperature Thermoelectric Behavior

(Submitted to Journal of Physics Condensed Matter)

F. Drymiotis, T. Drye, D. Rhodes, Q. Zhang, J. Lashey*, Y. Wang, S. Cawthorne, B. Ma, S. Lindsey and T. Tritt.

Department of Physics and Astronomy, Clemson University, Clemson SC 29634
*Los Alamos National Laboratory, Los Alamos New Mexico 87545

We have measured the thermal transport properties over the temperature range 1:8 K < T < 700 K of a two-phase alloy consisting of $AgSbTe_2$ and Ag_2Se in a 1:1 molar ratio. Typical electrical resistivity values at 700 K are in the range ~4 mOhm-cm $\leq\rho\leq$20 mOhm-cm, while low thermal conductivity values ($\kappa<1 Wm^{-1}K^{-1}$) were obtained. We find that the thermal conductivity of this crystalline alloy has temperature dependence strikingly similar to that of amorphous solids. Additionally the thermal conductivity, thermopower, and electrical resistivity are able to somewhat decouple due to the novel microstructure. This may make it possible to further optimize the thermoelectric performance by reducing the electrical resistivity. It is therefore envisaged that this system has potential as a high-performance bulk thermoelectric material.

1. Introduction

Sustainable energy research is currently on the forefront of scientific exploration thus a major effort is devoted to the development of new energy conservation and production techniques. Thermoelectric materials can play a significant part both in energy conservation and energy production, since they can convert wasted heat to useful electrical energy[1-3]. In automotive applications, thermoelectrics can be used to collect the wasted heat from the exhaust and return it to the vehicle, in order to power electrical components, thus lowering engine load and decreasing fuel consumption. Alternatively, hot-springs may be used to generate electrical power since they provide a natural temperature reservoir. For power generation applications, the dimensionless figure of merit *ZT* (defined as $\alpha^2T/\kappa\rho$ where α is the thermopower or Seebeck coefficient, ρ is the electrical resistivity and κ is the total thermal conductivity) should have its maximum value at temperatures at or above 400 ^oC. Very high values of *ZT* (> 2)have been

observed in thin films[4] but unfortunately thin films are not suitable for high temperature and large scale applications. Thus, the current challenge is achieving comparable values of *ZT* (>2) in bulk materials.

Synthesis of low-carrier concentration complex alloys appears to be the most promising path for discovering new highly-efficient bulk thermoelectric materials[5]. Complicated structures with large and complex unit cells give rise to low thermal conductivity. Additionally, the structural disorder may be manipulated to vary the values of the electrical resistivity and thermopower. An ideal scenario would be the formation of a complex alloy which behaves as PGEC[6] (Phonon Glass Electron Crystal) – i.e. an alloy which has the electronic properties of a crystalline system and the thermal transport behavior of a glass. Formation of complex multi-phase alloys is thus an intriguing and logical synthesis technique for generating a PGEC alloy. Depending on the relative volume of the phases, the disorder scale can be comparable to the wavelength of long wavelength phonons, consequently leading to very low thermal conductivity. The main problem of this approach is the effect of the disorder on the electrical resistivity. Large electrical resistivity values will diminish thermoelectric performance, so the challenge is determining the proper phases to be used in the synthesis of the multi-phase alloy. In this work we show that the 2-phase alloy formed by melting $AgSbTe_2$-Ag_2Se in a 1:1 molar ratio ($Ag_3SbSeTe_2$), is a PGEC material with the potential for very high thermoelectric performance. Both $AgSbTe_2$ and Ag_2Se are well known thermoelectric materials[7-14], but ,most importantly, they both have low thermal conductivity. The resulting 2-phase alloy has good electronic properties but, most notably, its thermal conductivity behavior is similar to the thermal conductivity behavior of amorphous materials.

2. Experimental

Ag, Cu, Sb, Te, Se with respective purities of 99.9999%, 99.9999%, 99.9999%, 99.9999% and 99.999% were placed in quartz tubes in stoichiometric ratios 3-x:x:2:1, with x= 0, 0.1, 0.2. The quartz tubes were then evacuated, sealed, and placed inside a box furnace. The samples were subsequently heated to 1000 ^{o}C where they were allowed to remain for 4 hours, before finally being allowed to cool down to 500 ^{o}C at a rate of

10^{o}C/hour, at which point the power to the furnace was turned off. The formed ingots were then removed from the quartz tubes and processed for measurement. The mass of each ingot was approximately 20 grams. All samples obtained were highly dense with good mechanical properties. The density of all samples was approximately $d\sim7.3\ gr/cm^3$.

The x-ray diffraction data was obtained using a commercial Rigaku® diffractometer and the SEM and EDX analysis were performed using the Hitachi S3400-N SEM. The high-temperature resistivity and thermopower data were obtained using the ULVAC-ZEM2® measuring system. The high-temperature thermal-conductivity values were deduced from the thermal diffusivity values obtained using the Netzsch LFA 457® laser flash apparatus using the relation $\kappa=DdC_P$, with D being the measured value of the thermal diffusivity, d the density and C_P the heat capacity at constant pressure. The value of ρ used in the calculations was the measured density at room temperature, and the value of C_P was taken to be the value of the DuLong Petit limit. The low-temperature thermal conductivity data was taken using a Quantum Design PPMS® at Los Alamos National Laboratory.

3. Results and Discussion

The x-ray diffraction data shows the presence of 2 phases (figure 1), a phase which crystallizes in the $AgSbTe_2$ rocksalt structure[12] (cF8, No 225) and a phase which crystallizes in the monoclinic α-Ag_2Te structure[15] (mP12, No 14) (figure 2). The average density of the samples is $d=7.30\ g/cm^3$ which is considerably higher than the density of $AgSbSe_2$ ($d=6.69\ g/cm^3$), slightly higher than the density of $AgSbTe_2$ ($d=7.12\ g/cm^3$) and significantly lower than the density of α-Ag_2Te ($d=8.21\ g/cm^3$).

Figure 1

The lattice parameter obtained from the x-ray (figure 1) data for the rocksalt phase is $a \sim 5.94\ A$ which lies between the lattice parameter of $AgSbSe_2$ ($a= 5.79\ A$) and the lattice parameter of $AgSbTe_2$ ($a= 6.07\ A$). Based on these values, it appears that the composition of the resulting mixture is Se-doped $AgSbTe_2$ and Se-doped- α-Ag_2Te. Preliminary EDX on 2 areas of the sample with distinct features, for the best performing Cu-doped sample, confirmed the existence of both Se-doped $AgSbTe_2$ and Se-doped

monoclinic Ag_2Te. The result is not surprising since it has been shown that Ag_2Te precipitates out of $AgSbTe_2$ during solidification[16], which implies that the monoclinic Ag_2Te, and not the orthorhombic Ag_2Se, is the thermodynamically stable second phase. Images of the phase reveal, as expected, 2 different phases which are uniformly distributed. The phase separation between the rocksalt structure (dark shade) and the monoclinic structure (light shade) is distinct (figure 3) and micro-fractures can been seen at the phase boundaries. These micro-fractures are likely due to the strain field between the two phases. Both phases seem to occupy the same volume.

Figure 2

The temperature behavior of the electrical resistivity (figure 4) is typical of some type of an activated process. This activated behavior is observed at high-temperatures while the room-temperature resistivity is dominated by intrinsic effects. We have not performed the low temperature electrical transport measurements but plan to do so in near term. The feature at *400 K* in the resistivity versus temperature data corresponds to the $\alpha \rightarrow \beta$ structural phase transition in the doped Ag_2Te. The resistivity decreases with increasing Cu concentration from a value of *11.8 mOhm-cm* for the x=0 sample to *3.3 mOhm-cm* for the best $\delta = 0.2$ sample. The resistivity values vary from sample to sample which is expected behavior in a complex alloy with low electronic energies.

Figure 3

The cooling profile, sample homogeneity and variations in stoichiometry, and the presence of micro-fractures are all factors which can substantially affect electronic transport. We should note that the samples that do not contain Cu, the resistivity and thermopower values change when the sample is annealed at *400 ^oC*. Adding Cu appears to stabilize the resulting structure and consequently eliminates the changes in the electrical transport and thermopower behavior caused by annealing.

Figure 4

In contrast to the resistivity, the thermopower of the stoichiometric and Cu-doped samples is extremely robust and does not vary significantly from sample to sample (figure 5). The thermopower shows n-type behavior at low temperatures and p-type

behavior at high temperatures. The transition from n- to p- type behavior coincides with the Ag_2Te $\alpha \rightarrow \beta$ structural phase transition. The value of the thermopower tends to converge for all the samples at $T \sim 700\ K$ and the value there is approximately $\alpha \sim 230\ \mu V/K$. The phase transition makes it difficult to discern the overall transport mechanism from the resistivity measurements, whether it would be hoping or semiconducting. However the large values of the resistivity would indicate a semiconducting behavior. Cu doping does not produce significant changes in the thermopower which implies that Cu doping does not noticeably affect the band structure. This is expected since Cu and Ag are isoelectronic. The most plausible explanation for this behavior is the presence of the observed micro-fractures. The concentration of micro-structures will presumably vary from sample to sample but it will have no effect on the thermopower since the band structure will remain unaltered. The electrical conductivity though will be affected since the micro-fractures will enhance electronic scattering and consequently increase the electrical resistivity.

Figure 5

The high temperature thermal conductivity behavior of this alloy is extremely interesting (figure 6). The thermal conductivity increases with increasing temperature and the thermal conductivity values for all compositions are very small. The thermal conductivity value for the stoichiometric composition (x=0) is $\kappa_{Total} = 0.7\ W/m\text{-}K$ at $700\ K$ while the thermal conductivity value for the x=0.1 alloy is approximately the same. A noticeable decrease is observed for the x=0.2 sample; $\kappa_{Total} = 0.6\ \ W/m\text{-}K$ at $700\ K$. The uncertainly in the thermal conductivity values is on the order of *7-8%.*

Figure 6

Surprisingly, the low-temperature thermal conductivity (figure 7) shows glass-like behavior. According to the x-ray diffraction data, this is a crystalline system, so the glass-like behavior is unexpected. The behavior presumably arises due to the large level of disorder which eliminates translational invariance. As a result, heat is transported through localized vibrations and consequently the lattice thermal conductivity is greatly reduced. The presence of localized vibrations typically gives rise to a $\kappa_{Phonon}\ \alpha\ T^2$

dependence of the thermal conductivity at very low temperatures[17-20]. A $\kappa_{Phonon} \alpha T$ dependence has also been observed at low temperatures in quartz[21, 22] and the bulk-metallic glass[23] $Ni_{59.5}Nb_{33.6}Sn_{6.9.}$ In this particular alloy, the low temperature thermal conductivity in the temperature range $1.8\ K \leq T \leq 3.5\ K$ (electronic contribution is negligible in this temperature range) varies linearly with temperature (inset of figure 7). A plateau can also be seen at a temperature $T \sim 4\ K$. The appearance of a plateau in the thermal conductivity is a prominent feature of amorphous solids and it is attributed to a rapidly decreasing phonon mean free path with the increasing frequency[24]. At higher temperatures, the increasing thermal conductivity is due to the electronic contribution. The electronic contribution can be calculated using the Wiedemann-Franz law ($\kappa_{electronic} = LoT/\rho$ with $Lo = 2.45 \times 10^{-8}\ (V/K)^2$. Using an average value for the resistivity $\rho = 1x10^{-4}$ Ohm-m we find that the electronic contribution to the thermal conductivity $\kappa_{electronic}=0.2\ W/m\text{-}K$ which implies that the lattice thermal conductivity is $\kappa_{lattice} = 0.4\ W/m\text{-}K$. The thermal conductivity values for both the stoichiometric and Cu-doped samples, are repeatable and do not vary significantly from sample to sample.

Figure 7

4. Conclusions

The electronic and thermal transport behavior of this 2-phase alloy make it an interesting candidate for high temperature thermoelectric applications. The thermopower and thermal conductivity depend very weakly on Cu concentration whereas the resistivity varies considerably. The apparent decoupling of the thermopower, thermal conductivity and resistivity gives us the ability to manipulate the alloy either through slight changes in composition and/or changes in the growth temperature profile, in order to minimize its electrical resistivity (changes in the growth temperature profile did not produce changes in the thermopower and thermal conductivity). Based on our initial measurements higher ZT values are possible if we are able to achieve lower values of resistivity by further control of the microstructure and the micro-fractures. More importantly, we have shown that a phonon glass can be realized in crystalline multi-phase alloys (PGEC), which

suggests that multi-phase alloys may be important candidates in our search for materials with very high-thermoelectric performance.

Acknowledgements

We would like to thank NSF-DMR-0905322 for the major support of this project. Part of the work at Clemson University is supported from DOE/EPSCoR Implementation Grant (#DE-FG02-04ER-46139), and SC EPSCoR cost sharing. The work at Los Alamos National Laboratory is supported by the US Department of Energy.

References

1 T. M. Tritt, *Thermoelectric materials 2000--the next generation materials for small-scale refrigeration and power generation applications : symposium held April 24-27, 2000, San Francisco, California, U.S.A* (Materials Research Society, Warrendale, Pa., 2001).

2 G. S. Nolas and Materials Research Society. Meeting, *Thermoelectric materials 2003--research and applications : symposium held December 1-3, 2003, Boston, Massachusetts, U.S.A* (Materials Research Society, Warrendale, Pa., 2004).

3 L. E. Bell, Science **321**, 1457 (2008).

4 R. Venkatasubramanian, E. Siivola, T. Colpitts, and B. O'Quinn, Nature **413**, 597 (2001).

5 G. J. Snyder and E. S. Toberer, Nature Materials **7**, 105 (2008).

6 G. S. Nolas, J. Poon, and M. Kanatzidis, Mrs Bulletin **31**, 199 (2006).

7 M. G. Ramazanzade, S. A. Aliyev, N. A. Verdiyeva, and A. M. Agayev, Izvestiya Vysshikh Uchebnykh Zavedenii Fizika, 27 (1981).

8 M. Ferhat and J. Nagao, Journal of Applied Physics **88**, 813 (2000).

9 C. Lee, Y. H. Park, and H. Hashimoto, Journal of Applied Physics **101** (2007).

10 H. A. Ma, T. C. Su, P. W. Zhu, J. G. Guo, and X. P. Jia, Journal of Alloys and Compounds **454**, 415 (2008).

11 H. Wang, J. F. Li, M. M. Zou, and T. Sui, Applied Physics Letters **93** (2008).

12 K. Wojciechowski, J. Tobola, M. Schmidt, and R. Zybala, Journal of Physics and Chemistry of Solids **69**, 2748 (2008).

13 F. F. Aliev, M. B. Jafarov, and V. I. Eminova, Semiconductors **43**, 977 (2009).

14 V. Jovovic and J. P. Heremans, Journal of Electronic Materials **38**, 1504 (2009).

15 P. Villars and L. D. Calvert, *Pearson's handbook of crystallographic data for intermetallic phases* (ASM International, Materials Park, OH, 1991).

16 J. D. Sugar and D. L. Medlin, Journal of Alloys and Compounds **478**, 75 (2009).

17 J. E. Graebner, B. Golding, and L. C. Allen, Physical Review B **34**, 5696 (1986).

18 C. C. Yu and J. J. Freeman, Physical Review B **36**, 7620 (1987).

[19] L. Gil, M. A. Ramos, A. Bringer, and U. Buchenau, Physical Review Letters **70**, 182 (1993).
[20] Y. K. Kuo, K. M. Sivakumar, C. A. Su, C. N. Ku, S. T. Lin, A. B. Kaiser, J. B. Qiang, Q. Wang, and C. Dong, Physical Review B **74** (2006).
[21] R. Berman, Proc. Roy. Soc. A **208**, 90 (1951).
[22] P. G. Klemens, Proc. Roy. Soc. A **208**, 108 (1951).
[23] Z. H. Zhou, C. Uher, D. H. Xu, W. L. Johnson, W. Gannon, and M. C. Aronson, Applied Physics Letters **89** (2006).
[24] K. Gianno, A. V. Sologubenko, M. A. Chernikov, H. R. Ott, I. R. Fisher, and P. C. Canfield, Physical Review B **62**, 292 (2000).

List of figures

Figure 1. X-ray diffraction data of $Cu_{0.2}Ag_{2.8}SbSeTe_2$. The dark circles correspond to the location of the $AgSbTe_2$ peaks.

Figure 2. The (a) rocksalt $AgSbTe_2$ structure and (b) the monoclinic Ag_2Te structure (index vector 0 1 0). Dark spheres correspond to Ag and Sb locations and grey spheres correspond to Te locations.

Figure 3. SEM image (top) shows the presence of both the cubic $AgSbTe_2$ (dark shade) and monoclinic Ag2Te (light shade). Notice the presence of micro-fractures that exist between the two phases.

Figure 4. Electrical resistivity versus temperature of $Cu_xAg_{3-x}SbSeTe_2$ for x=0, 0.1 and 0.2.

Figure 5. Thermopower versus temperature of $Cu_xAg_{3-x}SbSeTe_2$ for x=0, 0.1 and 0.2.

Figure 6. High temperature thermal conductivity of $Cu_xAg_{3-x}SbSeTe_2$ for x=0, 0.1 and 0.2 versus temperature.

Figure 7. Low temperature thermal conductivity $Cu_{0.2}Ag_{2.8}SbSeTe_2$ plotted in log-log scale. The thermal conductivity plateau can be seen at ~ 4 K. The inset (linear scale) shows the linear dependence of the thermal conductivity on temperature.

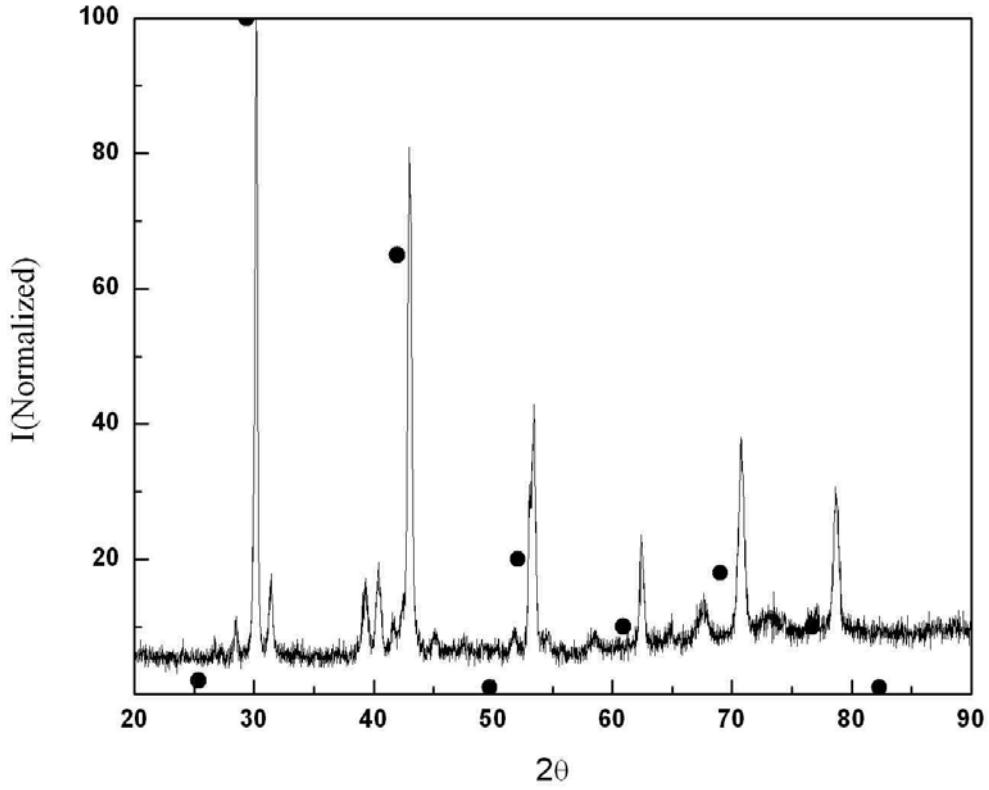

Figure 1.

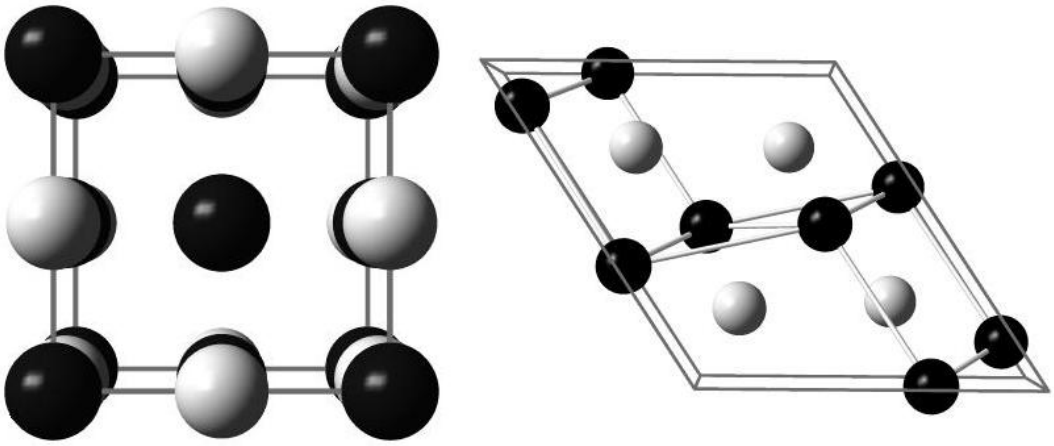

Figure 2.

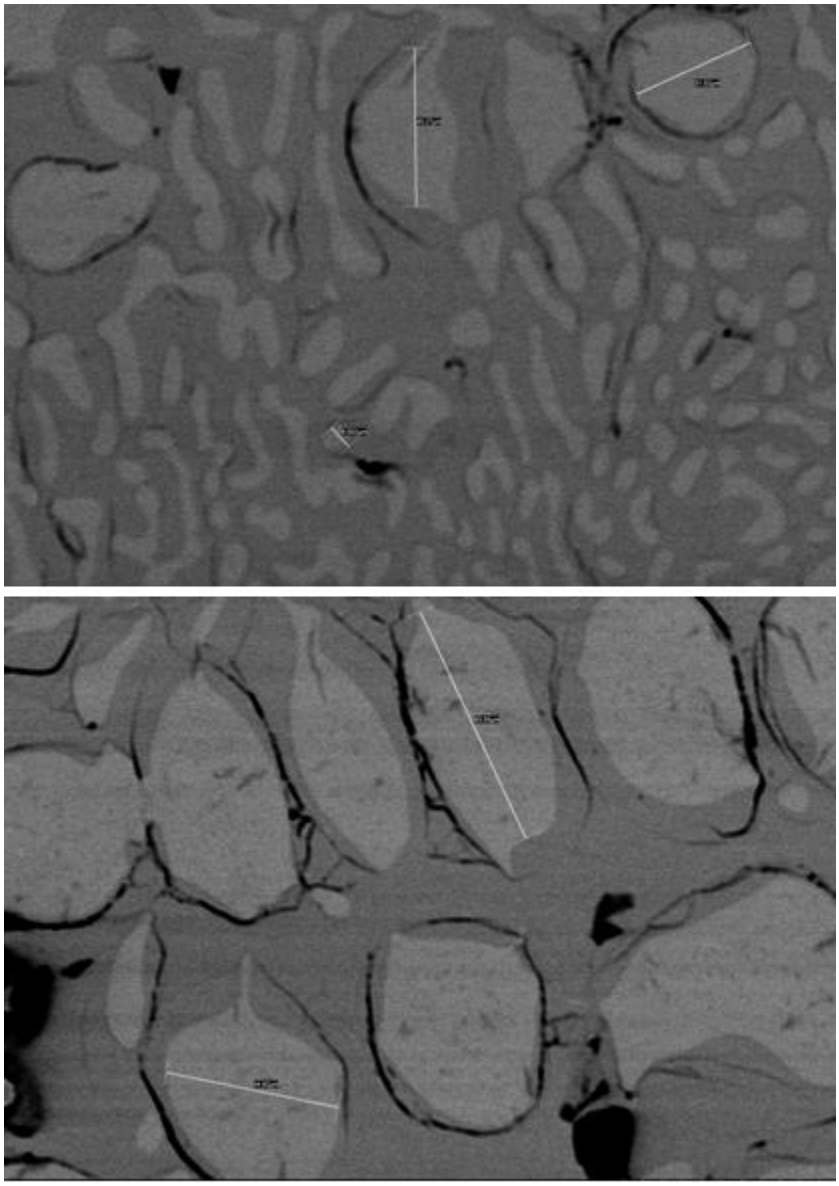

Figure 3.

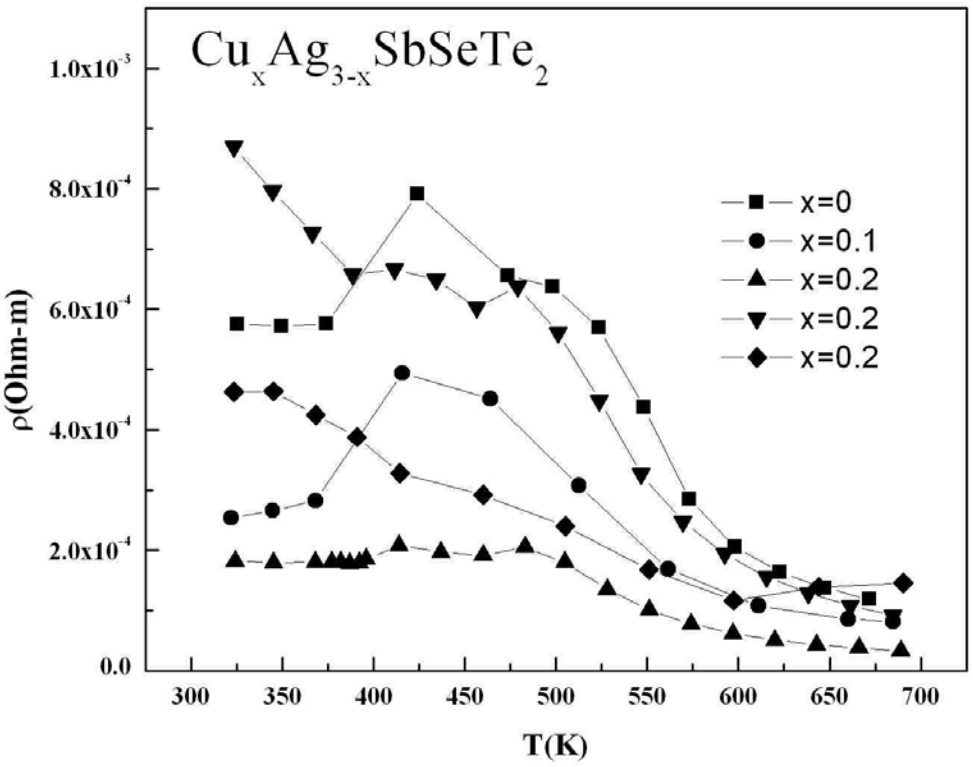
Cu$_x$Ag$_{3-x}$SbSeTe$_2$
1.0x10^{-3}
8.0x10^{-4}
6.0x10^{-4}
4.0x10^{-4}
2.0x10^{-4}
0.0
ρ(Ohm-m)
300
350
400
450
500
550
600
650
700
T(K)
x=0
x=0.1
x=0.2
x=0.2
x=0.2

Figure 4.

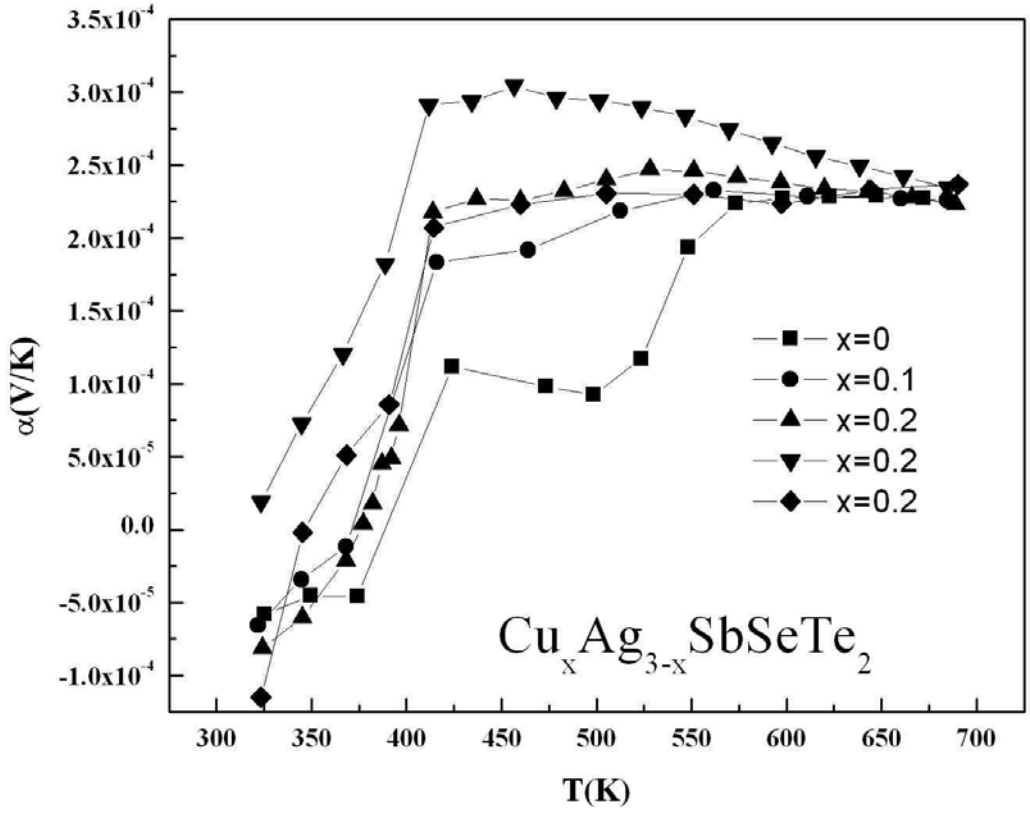
3.5x10-4
3.0x10-4
2.5x10-4
2.0x10-4
1.5x10-4
1.0x10-4
5.0x10-5
0.0
-5.0x10-5
-1.0x10-4
α(V/K)
300
350
400
450
500
550
600
650
700
T(K)
x=0
x=0.1
x=0.2
x=0.2
x=0.2
CuxAg3-xSbSeTe2

Figure 5.

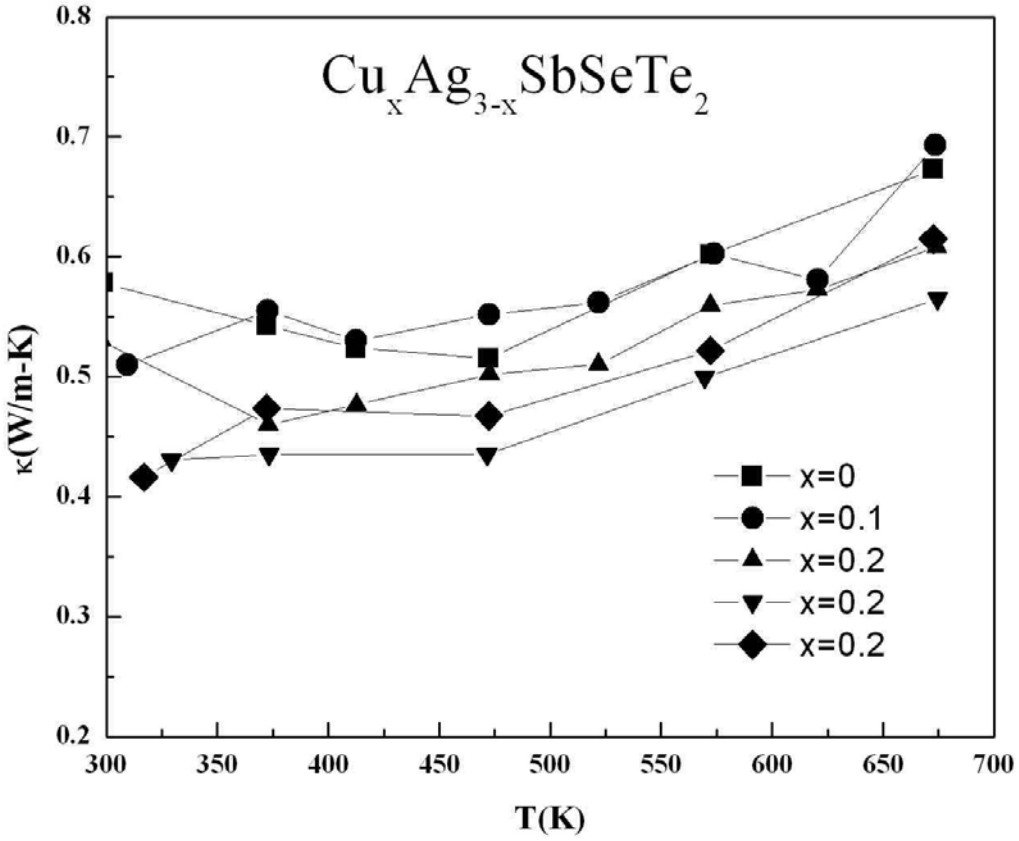
Cu$_x$Ag$_{3-x}$SbSeTe$_2$
κ(W/m-K)
T(K)
0.8
0.7
0.6
0.5
0.4
0.3
0.2
300
350
400
450
500
550
600
650
700
x=0
x=0.1
x=0.2
x=0.2
x=0.2

Figure 6.

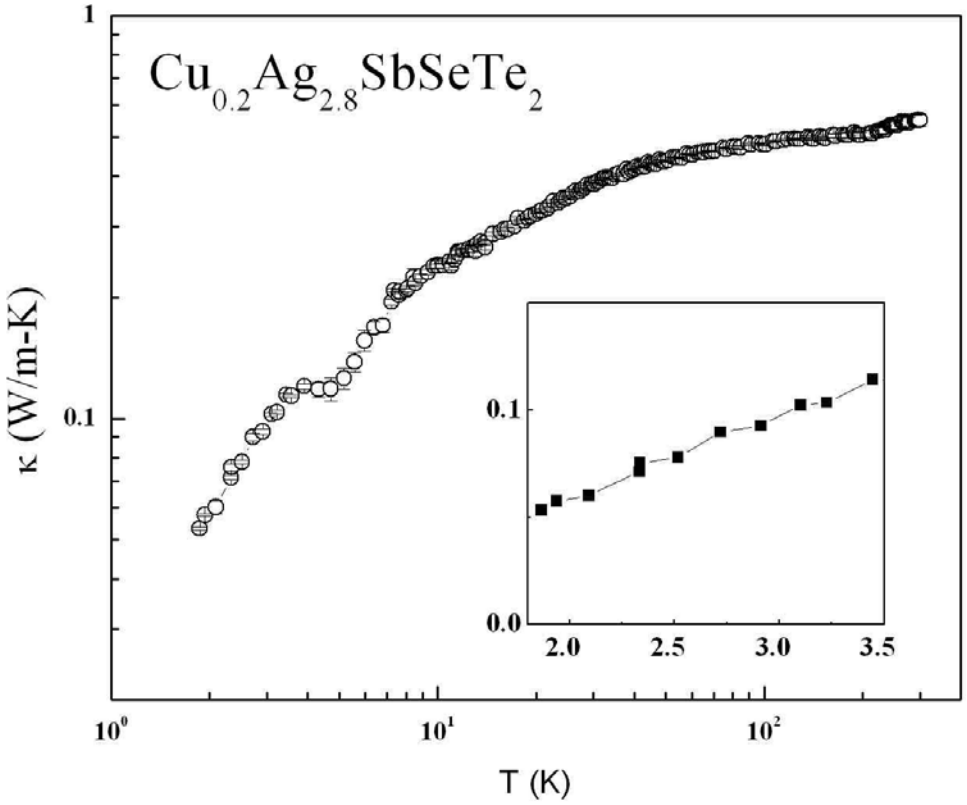

Figure 7.

REFERENCES

1. http://www.thermoelectrics.com/go.html
2 terry tritt. Science
3 T. M. Tritt, Thermoelectric materials 2000--the next generation materials for small-scale refrigeration and power generation applications : symposium held April 24-27, 2000, San Francisco, California, U.S.A (Materials Research Society, Warrendale, Pa., 2001), p. 1 v. (various pagings).
4 Seebeck, T.J., 1822, Magnetiche Polarisation derMetalle und Erzedurch Temperature Differenz. Abband Deut. Akad. Wiss. Berlin
5 Peltier, J.C., 1834, Nouvelles experiences sur la calorecete des courans electriques. Ann. Chem
6 Thomson, W., 1851, On a mechanical theory of thermoelectric currents, Proc. Roy. Soc. Edinburgh, 91-98
7. D.M. Rowe, Thermoelectrics Handbook:macro to nano. Page from 1-3 to 1-4
8. D.M. Rowe, Thermoelectrics Handbook:macro to nano. Page from 1-4 to 1-7
9. modern thermoelectric, D.M. Rowe and C.M. Bhandari
10. D.M. Rowe, Thermoelectrics Handbook:macro to nano. Page from 1-7 to 1-9
11 Fivos R Drymiotis, Tyler B Drye, Yisha Wang, Jian He, Daniel Rhoades, Kimberly Modic, Samantha Cawthorne, Terry Tritt, Structure formation and very low thermal conductivity in dense Pb:Te:Ag:Se mixtures
12 F. Drymiotis, T. Drye, D. Rhodes, Q. Zhang, J. Lashey, Y. Wang, S. Cawthorne, B. Ma, S. Lindsey and T. Tritt, Glassy Thermal Conductivity in the 2-phase CuxAg3-xSbSeTe2 alloy and High-Temperature Thermoelectric Behavior
13 Complex & Advanced Materials Lab,
http://virtual.clemson.edu/groups/TMRL/Contact.html
14. A.L. Pope, B. Zawilski, and T.M.Tritt, Cryogenics 41(2001) 725-731
15 Model ZEM-2 Seebeck Coefficient Measuring SystemInstruction Mannual
16 A.L. Pope, R.T. Littleton IV, T.M. Tritt, Rev. Sci. Instrum. 72 (2001) 3129-3131
17 Electron Microscope Facility at Clemson University,
http://www.clemson.edu/electronmicroscope/
18 Operating Instructions Micro-Flash-Apparatus LFA 457
19 M. Kobayashi, Review on Structural and Dynamic Properties of Silver Chalcogenides, Solid State Ionics 39, 121 (1990)
20 T. B. Massalski, H. Okamoto, and ASM International., Binary alloy phase diagrams (ASM International, Materials Park, Ohio, 1990), pp. 3 v. (xiv)
21 K. Wojciechowski, J. Tobola, M. Schmidt, and R. Zybala, Journal of Physics and Chemistry of Solids 69, 2748 (2008)
22 P. Villars and L. D. Calvert, Pearson's handbook of crystallographic data for intermetallic phases (ASM International, Materials Park, OH, 1991)
23 K. Wojciechowski, J. Tobola, M. Schmidt, and R. Zybala, Journal of Physics and Chemistry of Solids 69, 2748 (2008).
24 F. F. Aliev, M. B. Jafarov, and V. I. Eminova, Semiconductors 43, 977 (2009)
25 V. Jovovic and J. P. Heremans, Journal of Electronic Materials 38, 1504 (2009)

26 P. Villars and L. D. Calvert, Pearson's handbook of crystallographic data for intermetallic phases (ASM International, Materials Park, OH, 1991)
27 J. D. Sugar and D. L. Medlin, Journal of Alloys and Compounds 478, 75 (2009)
28 J. E. Graebner, B. Golding, and L. C. Allen, Physical Review B 34, 5696 (1986)
29 C. C. Yu and J. J. Freeman, Physical Review B 36, 7620 (1987)
30 L. Gil, M. A. Ramos, A. Bringer, and U. Buchenau, Physical Review Letters 70, 182 (1993)
31 Y. K. Kuo, K. M. Sivakumar, C. A. Su, C. N. Ku, S. T. Lin, A. B. Kaiser, J. B. Qiang, Q. Wang, and C. Dong, Physical Review B 74 (2006)
32 R. Berman, Proc. Roy. Soc. A 208, 90 (1951)
33 P. G. Klemens, Proc. Roy. Soc. A 208, 108 (1951)
34 Z. H. Zhou, C. Uher, D. H. Xu, W. L. Johnson, W. Gannon, and M. C. Aronson, Applied Physics Letters 89 (2006)
35 K. Gianno, A. V. Sologubenko, M. A. Chernikov, H. R. Ott, I. R. Fisher, and P. C. Canfield, Physical Review B 62, 292 (2000)